

Impacts of Forced and Internal Climate Variability on Changes in Convective Environments Over the Eastern United States

Megan Elizabeth Franke¹, James Wilson Hurrell¹, Kristen Rasmussen¹, and Lantao Sun¹

¹Colorado State University

January 24, 2023

Abstract

Hazards from convective weather pose a serious threat to the continental United States (CONUS) every year. Previous studies have examined how future projected changes in climate might impact the frequency and intensity of severe weather using simulations with both convection-permitting regional models and coarser climate and Earth system models. However, many of these studies have been limited to single representations of the future climate state with little insight into the uncertainty of how the population of convective storms may evolve. To thoroughly explore this aspect, a large ensemble of Earth system model simulations was implemented to investigate how forced responses in large-scale convective environments might be modulated by internal climate variability. Daily data from an ensemble of 50 simulations with the most recent version of the Community Earth System Model was used to examine changes in the severe weather environment over the eastern CONUS during boreal spring from 1870-2100. Results indicate that forced changes in convective environments were small between 1870 and 1990, but throughout the 21st century, convective available potential energy and atmospheric stability (convective inhibition) is projected to increase while 0-6 km vertical wind shear decreases. Internal climate variability can either significantly enhance or suppress these forced changes. The time evolution of bivariate distributions of convective indices illustrates that future springtime convective environments over the eastern CONUS will be characterized by relatively less frequent, less organized, but deeper, more intense convection. Future convective environments will also be less supportive of the most severe convective modes and associated hazards.

1 **Impacts of Forced and Internal Climate Variability on**
2 **Changes in Convective Environments Over the Eastern**
3 **United States**

4 **Megan E. Franke¹, James W. Hurrell¹, Kristen L. Rasmussen¹, Lantao Sun¹**

5 ¹Colorado State University

6 **Key Points:**

- 7 • The signal of climate change in large-scale convective environments over the U.S.
8 emerges from the internal variability in the late 1990's.
9 • Future convective environments over the eastern U.S. will be supportive of less fre-
10 quent, less organized, but more intense storms.
11 • Large-scale internal climate variability could significantly enhance or suppress the
12 changes due to anthropogenic climate change.

Corresponding author: Megan E. Franke, megan.franke@colostate.edu

Abstract

Hazards from convective weather pose a serious threat to the continental United States (CONUS) every year. Previous studies have examined how future projected changes in climate might impact the frequency and intensity of severe weather using simulations with both convection-permitting regional models and coarser climate and Earth system models. However, many of these studies have been limited to single representations of the future climate state with little insight into the uncertainty of how the population of convective storms may evolve. To thoroughly explore this aspect, a large ensemble of Earth system model simulations was implemented to investigate how forced responses in large-scale convective environments might be modulated by internal climate variability. Daily data from an ensemble of 50 simulations with the most recent version of the Community Earth System Model was used to examine changes in the severe weather environment over the eastern CONUS during boreal spring from 1870-2100. Results indicate that forced changes in convective environments were small between 1870 and 1990, but throughout the 21st century, convective available potential energy and atmospheric stability (convective inhibition) is projected to increase while 0-6 km vertical wind shear decreases. Internal climate variability can either significantly enhance or suppress these forced changes. The time evolution of bivariate distributions of convective indices illustrates that future springtime convective environments over the eastern CONUS will be characterized by relatively less frequent, less organized, but deeper, more intense convection. Future convective environments will also be less supportive of the most severe convective modes and associated hazards.

Plain Language Summary

Understanding to what extent climate change will alter severe weather is critical for planning and resilience. Moreover, natural variations in climate could either enhance or suppress climate change signals, so documenting the range of equally plausible future outcomes is important. Utilizing a large number of simulations from a climate model, we document projected changes in large-scale atmospheric conditions critical to severe weather from both climate change and natural variability. The impact of climate change on these environments became apparent late in the 20th century and will likely strengthen over the coming decades. Convective environments over the eastern U.S. will increasingly be supportive of less frequent, less organized, but more explosive storms due to increases in mid-level stability and positively buoyant energy, but slight decreases in vertical wind shear. However, such changes may be significantly modified by natural climate variability, resulting in a wide range of possible outcomes.

1 Introduction and Motivation

Few places around the globe experience extreme severe weather like the United States (U.S.). Particularly over the central and eastern U.S., the peak in severe weather is largely due to synoptic-scale interactions with the Rocky Mountains. During the boreal spring season, the Bermuda High, as well as the nocturnal Great Plains Low-Level Jet (GPLLJ), enhances a southerly flow of warm, moist air from the Gulf of Mexico into the Great Plains (Pitchford & London, 1962; Higgins et al., 1997; W. Li et al., 2011). This moist air, trapped by the mountains to the west, creates a strong gradient between the dry, western desert air and provides the necessary ingredients for high convective energy downstream. In addition, the terrain of the Rockies helps to produce a mid-level capping inversion as the hot, dry, mixed-layer air is advected off the elevated plateaus, which can then be further enhanced as the climatological westerly flow aloft descends the lee-side of the mountains (Carlson et al., 1983). This inversion suppresses convective activity and further facilitates the daily accumulation of convective energy increasing to very high levels. If the inversion is then broken, enhanced lifting and deep convection can occur.

63 In the year 2021 alone, 20 destructive meteorological events occurred in the U.S.
64 each resulting in \$1 billion or more of damages. Eleven of these events were due to se-
65 vere weather and included hazards such as tornadoes, large hail, and strong winds (NCEI,
66 2021). Records from the National Climatic Data Center indicate that, over the last decade,
67 the occurrence of billion-dollar severe weather events has more than doubled. Addition-
68 ally, the Intergovernmental Panel on Climate Change (IPCC) has noted with high confi-
69 dence that models consistently project changes in climate that support an increase in
70 the frequency and intensity of severe weather (IPCC, 2021). As temperatures increase
71 due to enhanced greenhouse gas concentrations, the air-column moisture content also in-
72 creases, thus leading to an increase in convective available potential energy - a key in-
73 gredient for the development of severe weather. In the current climate, hazards associ-
74 ated with severe storms already threaten lives, infrastructure, and food and water sup-
75 plies within the U.S. and elsewhere. With this in mind, an improved understanding of
76 the causes of both near-term and longer-timescale variability in severe weather could aid
77 in improving the accuracy of future predictions, as well as enhance resilience to severe
78 weather outbreaks.

79 Due to their relatively small scale and intermittent occurrence, observing and col-
80 lecting homogeneous records of severe weather events is difficult, especially when these
81 events occur in relatively unpopulated or rural areas (Johns & Doswell, 1992; Brooks et
82 al., 2003). To partially offset the lack of direct, long-term, and reliable observations of
83 severe storm events, the severe weather research community has developed convective
84 indices and covariate proxies that represent the thermodynamic and kinematic compo-
85 nents of the local storm environment and are indicative of conditions favorable for se-
86 vere weather events (Ludlam, 1963; E. N. Rasmussen & Blanchard, 1998; Craven & Brooks,
87 2004). Consideration of these diagnostic variables can aid in determining the historical
88 occurrence and future probability of severe weather, including the frequency, intensity,
89 and type, or mode, of convection.

90 Convective Available Potential Energy (CAPE) is a measure of the potential en-
91 ergy available for upward vertical motion in a storm environment, while Convective In-
92 hibition (CIN) is indicative of the boundary layer stability, which inhibits upward ver-
93 tical motion. Considerable prior research has investigated both the recent historical cli-
94 matology as well as projections of the future evolution of these parameters. In general,
95 these studies have shown that boreal spring CAPE is expected to increase substantially
96 over the eastern continental U.S. (CONUS) by the end of the 21st century, largely as a
97 result of an increase in specific humidity and warmer temperatures (e.g., Trapp et al.,
98 2007, 2009; Diffenbaugh et al., 2013; Seeley & Romps, 2015; Hoogewind et al., 2017; K. L. Ras-
99 mussen et al., 2017; Chen et al., 2020; Lepore et al., 2021). Although less explored, the
100 spatiotemporal evolution of boreal spring CIN is also consistent among previous stud-
101 ies, with increasing boundary layer stability (increasing CIN magnitudes) by 2100, par-
102 ticularly over the central CONUS (e.g., Hoogewind et al., 2017; K. L. Rasmussen et al.,
103 2017; Chen et al., 2020; Lepore et al., 2021). While many of these studies have utilized
104 large-scale climate models to explore future changes in these convective indices, others
105 have taken a different approach by applying dynamical downscaling or the pseudo-global
106 warming approach (Hoogewind et al., 2017; Chen et al., 2020). For example, K. L. Ras-
107 mussen et al. (2017) analyzed high-resolution convection-permitting simulations (Liu et
108 al., 2017) using the regional Weather Research and Forecasting model (WRF; Skamarock
109 et al., 2008) at 4 km resolution forced with ERA-Interim Reanalysis plus a climate change
110 perturbation from climate model simulations to investigate how CAPE, CIN, and their
111 subsequent convective populations may change in the future. In particular, they calcu-
112 lated end-of-century monthly anomalies of CAPE and CIN relative to the historical cli-
113 matology (1976-2005) using a 19-model ensemble-mean from phase 5 of the Coupled Model
114 Intercomparison Project (CMIP5; Taylor et al., 2012) under a strong, future emissions
115 scenario. Their results are broadly consistent with the aforementioned studies, with in-
116 creases projected in spring and summer CAPE and increasing magnitudes of CIN (in-

117 creased stability) over the eastern CONUS. Such findings suggest that in the future, weak
118 to moderate storms will be less frequent because of increased stability, but the most in-
119 tense storms will become more numerous (K. L. Rasmussen et al., 2017).

120 In contrast, there is less agreement on projected end-of-century changes in tropo-
121 spheric wind shear, which is a key factor for storm organization, longevity, and severe
122 weather development. For instance, Trapp et al. (2007), Diffenbaugh et al. (2013), and
123 Ting et al. (2019) used a variety of Earth system models with RCP8.5 forcing and found
124 a robust swath of decreasing wind shear over most of the CONUS during the boreal spring
125 season, while Hoogewind et al. (2017) and Lepore et al. (2021) both found increasing wind
126 shear over the western and central U.S. with decreasing shear over the eastern U.S. by
127 2100 also using Earth system models.

128 While changes in individual convective indices are useful for analyzing specific char-
129 acteristics of severe storms, integrated measures of changes in storm environments, such
130 as the product of CAPE and the wind shear between the surface and 6-km (S06), can
131 provide a more complete spatiotemporal description of the convective environment. By
132 definition, CAPES06 considers both the thermodynamic energy and the kinematic mo-
133 tion in a storm environment. As a result, increases in this variable could signify an in-
134 crease in the frequency of significant severe storms relative to non-severe storms (E. N. Ras-
135 mussen & Blanchard, 1998; Brooks et al., 2003; Brooks, 2009). The historical climatol-
136 ogy of warm-season CAPES06 produces a large-scale, spatially coherent pattern over the
137 eastern CONUS, reflecting the climatology of the CAPE index (Brooks et al., 2003; F. Li
138 et al., 2020). Simulations of future projections suggest that CAPES06 will mirror changes
139 in CAPE. For instance, Seeley and Romps (2015) used a subset of climate models from
140 the CMIP5, chosen based on their ability to reproduce a radiosonde climatology of se-
141 vere storm environments, to compare 21st century changes in the frequency of environ-
142 ments favorable for severe weather using a CAPES06 threshold. In general, all four mod-
143 els produced changes for end-of-century CAPES06 that showed consistent spatial pat-
144 terns with increases over the southern and central U.S. ranging from 50 to 180% of the
145 historical climatology (Seeley & Romps, 2015).

146 Another approach has been to consider combinations of convective indices to de-
147 termine the Number of Days with SEVere weather environments (NDSEV; Brooks et al.,
148 2003). Previous studies agree that NDSEV will increase over much of the U.S. during
149 the boreal spring season, but differences exist in the projected magnitudes of the increases.
150 For instance, Trapp et al. (2007, 2009) and Diffenbaugh et al. (2013) find an increase of
151 ~ 3 days per season over the central and eastern CONUS by 2100 utilizing an Earth sys-
152 tem model, whereas Hoogewind et al. (2017) found an increase of ~ 10 days per season
153 using a dynamical downscaling approach. Such discrepancies are likely a consequence
154 of varying definitions used for the NDSEV parameter, contrasting time periods between
155 the studies, as well as model grid-spacing and emission scenario differences.

156 The aforementioned studies have provided valuable insights and have set the founda-
157 tion for the types of changes that are likely to be experienced in future convective en-
158 vironments during the boreal spring over the U.S. However, they primarily use either a
159 small number of simulations from a single model, short integration periods (~ 30 years),
160 or multi-model ensemble means with different emission scenarios and other model vari-
161 ations to compare changes in convective environments due to anthropogenic forcing. An
162 additional and important perspective can be gained by utilizing a large ensemble approach
163 from a single model, whereby many simulations of the future are run under the same ra-
164 diative forcing scenario but are started from slightly different initial conditions. The sig-
165 nificance of this approach arises from the presence of unpredictable, internal (or natu-
166 ral) climate variability, which results in a range of possible future outcomes, all of which
167 can be considered a possible reality (e.g., Deser et al., 2012a). Internal variability is one
168 of the largest factors of unavoidable uncertainty in regional climate projections and can
169 either enhance or suppress a forced signal (Deser, 2020). It is important to note that each

170 simulation in a large ensemble contains a common response to the radiative forcing su-
171 perimposed upon a different sequence of internal variability. In general, internal climate
172 variability is larger in the extra-tropics than in the tropics and is relatively stronger com-
173 pared to forced variability when examining climate change several decades into the fu-
174 ture (Hawkins & Sutton, 2009; Deser et al., 2012a; Milinski et al., 2020), as has been done
175 here.

176 Sub-seasonal to decadal variability is often associated with leading modes of cli-
177 mate variability. A handful of studies have examined the relationship between severe weather
178 and modes of climate variability such as the El Niño Southern Oscillation (ENSO; Lee
179 et al., 2013; Allen et al., 2015) and the Madden Julian Oscillation (MJO; Thompson &
180 Roundy, 2013). Allen et al. (2015) found that fewer tornado and hail events occur over
181 the central U.S. during El Niño events than during La Niña events. Thompson and Roundy
182 (2013) showed that violent tornado outbreaks in the months March-May are more than
183 two times more frequent during the second phase of the Real-time Multivariate MJO (RMM)
184 index than during any other phases or during MJO inactivity. These results are criti-
185 cal in helping to both better understand the patterns of severe weather outbreaks as well
186 as improve the skill for long-range seasonal predictions of severe weather events (Allen
187 et al., 2015). However, how low-frequency, unforced climate variability modulates the
188 convective mode (i.e. frequency and storm type), as well as the thermodynamic and kine-
189 matic environment critical for severe weather, has not been examined extensively to date,
190 even though it is likely an important influence regionally.

191 As such, this study builds on the previous literature, specifically by taking advan-
192 tage of a recently released large ensemble of simulations from the Community Earth Sys-
193 tem Model version 2.0 (CESM2; Danabasoglu et al., 2020), hereafter referred to as the
194 CESM2-LE (Rodgers et al., 2021). Leveraging the CESM2-LE, which extends from 1870-
195 2100, allows us to evaluate the temporal evolution of convective environments over a much
196 longer, continuous-time record than has been examined before. Further, it allows us to
197 robustly examine both the forced variability due to anthropogenic climate change, as well
198 as the possible role of internal variability in modulating the forced signal over the com-
199 ing decades. To our knowledge, these aspects related to severe weather environments over
200 the U.S. have yet to be rigorously examined, and thus represent a novel aspect of the
201 current study. An increased understanding of the possible combined effects of forced and
202 internal variability on convective environments is important for ensuring that climate
203 adaptation policies are based on the most complete, scientific information available (Deser,
204 2020; Mankin et al., 2020).

205 **2 Methodology**

206 We utilize simulation data from the CESM (Hurrell et al., 2013; Danabasoglu et
207 al., 2020). The open-source CESM is unique in that it is both developed and applied to
208 scientific problems by a large community of researchers. It is a critical infrastructure for
209 the U.S. climate research community and is principally funded by the National Science
210 Foundation (NSF) and managed by the U.S. National Center for Atmospheric Research
211 (NCAR). Simulations performed with the CESM have made many significant contribu-
212 tions to climate research, ranging from paleoclimate applications (e.g., Otto-Bliesner et
213 al., 2016) to contributions to the North American Multi-Model Ensemble (NMME; Kirt-
214 man et al., 2014) seasonal forecasting effort led by the National Oceanic and Atmospheric
215 Administration (NOAA). Simulations with CESM have also been used extensively in both
216 national and international assessments of climate science, including substantial contri-
217 butions to version 6 of the CMIP (CMIP6; Eyring et al., 2016). The salient point is that
218 CESM provides the broader academic community with a core modeling system to inves-
219 tigate a diverse set of earth system interactions across multiple time and space scales.

220

2.1 Model Information and Data

221

222

223

224

225

226

227

228

229

230

231

232

233

234

235

236

237

238

Daily data for specific humidity, column air temperature, near-surface (10-meter) wind speed, zonal and meridional winds, and geopotential heights were obtained from a large ensemble (LE) produced with the coupled CESM2 (Danabasoglu et al., 2020). The CESM2-LE uses the Community Atmosphere Model version 6 (CAM6), which is a ‘low-top’ model consisting of 32 vertical levels (a relatively coarse stratospheric representation) and a nominal 1° (1.25° in longitude and 0.9° in latitude) spatial resolution. To study the temporal evolution of the severe weather environment over the CONUS during boreal spring, 50 ensemble members were analyzed spanning 1870-2100. Each ensemble member used CMIP6 forcings over the historical record and a future (2015-2100) forcing of SSP3-7.0 (Rodgers et al., 2021), a medium-high emissions scenario resulting in approximately 7.0 Wm^{-2} in radiative forcing by the end of the 21st century (O’Neill et al., 2016; IPCC, 2021). This level of forcing is currently a policy-relevant target, and it is a more moderate forcing scenario than those analyzed in most of the aforementioned studies that have examined future changes in convective indices. An ensemble of this size and duration with a CMIP6 generation Earth system model provides an unprecedented opportunity to investigate the long-term evolution of large-scale convective environments, how it is impacted by forced variability, and to what extent the latter is influenced by internal climate variability.

239

2.2 Convective Parameters

240

241

242

243

244

245

246

247

248

249

The CESM2-LE simulations were used to compute several parameters to quantify the thermodynamic and kinetic characteristics of the large-scale storm environment across the U.S. Closely associated with the potential occurrence of deep convection is CAPE (Jkg^{-1}) (Doswell & Rasmussen, 1994; Riemann-Campe et al., 2009). This thermodynamic parameter is formally defined as the vertical integral of buoyancy from the level of free convection (LFC) to the equilibrium level, making it suitable to diagnose conditional instability and potential updraft strength (Holton & Hakim, 2013). We have chosen to use the most-unstable CAPE in the lowest 3000 meters to ensure that our analysis captures potentially elevated convection, as well as the maximum instability (Rochette et al., 1999).

250

251

252

253

254

255

256

257

The CIN (Jkg^{-1}) is equal to the negative buoyancy, or the negative work done by the atmospheric boundary layer as a parcel ascends from the surface, through the stable layer, and to the LFC (Colby, 1984; E. N. Rasmussen & Blanchard, 1998; Riemann-Campe et al., 2009). It is routinely analyzed to evaluate the stability of the local atmosphere and the potential suppression of convective motions. As CIN is the amount of energy an air parcel needs to overcome in order to reach the LFC, it is commonly referred to as a negative value (i.e., more negative values mean more convective inhibition or more stability), but will be discussed here as changes in magnitude.

258

259

260

261

262

263

264

265

266

267

268

269

270

To explore the kinematic components of the convective environment, we used the difference in the bulk vertical wind shear from 10 meters above ground level to 6-km (~ 525 hPa) altitude, known as S06 (ms^{-1}). Past work suggests that while lower-level wind shear is important for tornadic environments, S06 is one of the best indices for determining storm type and organization (E. N. Rasmussen & Blanchard, 1998; Weisman & Rotunno, 2000; Brooks et al., 2003). Large values of S06 are indicative of stronger mid-level rotation such as single-celled thunderstorms. In addition, higher S06 allows for increased organization for storm dynamics such as a tilted updraft, which is necessary to displace the area of upward vertical motion from the downward vertical motion. This increases the potential for the storm to form a mesocyclone and develop into a supercell, which is typically accompanied by severe weather hazards. Sufficient S06 is also essential for multi-cell organized systems, such as squall lines, as it helps to counteract the low-level circulation induced by the cold pool (Rotunno et al., 1988). As a cold pool is produced

271 by evaporative cooling near the surface, new cells are triggered along the gust front. The
 272 triggering and subsequent growth of these new cells are highly dependent on the amount
 273 of low-level wind shear, making it crucial to the longevity of a multi-cellular organized
 274 system.

275 A covariate convective index used here is the product of CAPE and S06, or CAPES06
 276 (m^3s^{-3}). Previous research has demonstrated the effectiveness of CAPES06 to help dis-
 277 criminate between significant severe storms and less severe storms (E. N. Rasmussen &
 278 Blanchard, 1998; Craven et al., 2002; Brooks et al., 2003; Brooks, 2009; Seeley & Romps,
 279 2015). As CAPES06 takes into account two of the most necessary components for con-
 280 vection, the thermodynamic energy and the vertical kinematic structure, high values of
 281 this parameter are indicative of increased storm organization and higher updraft veloc-
 282 ities. Historically, soundings from days with the most severe storms exhibited high val-
 283 ues in this index (e.g., E. N. Rasmussen & Blanchard, 1998; Brooks et al., 2003; Brooks,
 284 2009).

285 Finally, to convey the integrated effects of the convective indices, changes in ND-
 286 SEV are also examined. Following the definitions used in past studies (Brooks et al., 2003;
 287 Trapp et al., 2007; Gensini & Ashley, 2011; Hoogewind et al., 2017), a day is counted
 288 as a severe weather day when $\text{CAPE} \geq 100 \text{ Jkg}^{-1}$, $\text{CIN} \geq -100 \text{ Jkg}^{-1}$, $\text{S06} \geq 5 \text{ ms}^{-1}$,
 289 and $\text{CAPES06} \geq 10,000 \text{ m}^3\text{s}^{-3}$. Then, the sum of the number of days throughout the
 290 boreal spring season that meet the criteria are obtained to provide an estimate of the
 291 potential number of severe weather days per season.

292 This study will focus primarily on the eastern CONUS region outlined in Fig. 1,
 293 which is a highly active region for intense convection. Note, however, that the ocean re-
 294 gions are masked from the analysis so that the focus is on convective indices over land
 295 only. We define the spring season as March through June (MAMJ), as this period cap-
 296 tures the months when storms are most frequent and violent over the eastern CONUS
 297 (Kelly et al., 1985; Brooks et al., 2003; Gensini & Ashley, 2011; F. Li et al., 2020). Later
 298 into the summer season, the temperature and moisture gradients in this region are weaker,
 299 and the jet-stream begins to shift north, resulting in an overall northward shift in con-
 300 vective activity.

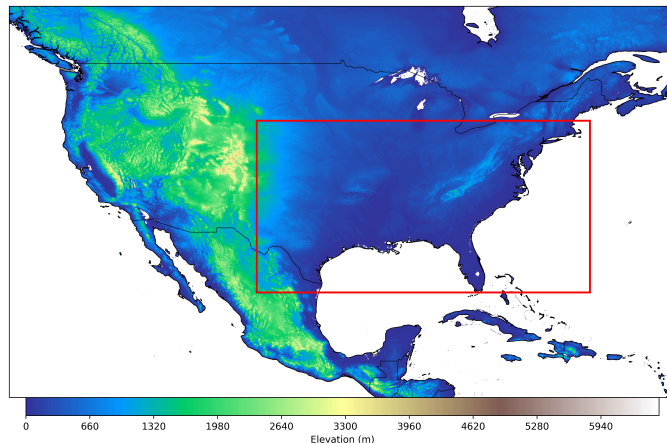


Figure 1. Red box highlights the eastern CONUS domain used for this study. Latitude bounds are between (25°N and 43°N) and longitude bounds are between (-104°W, -69°W).

301

2.3 Verification

302

303

304

305

306

307

308

309

310

311

312

313

314

315

316

317

318

319

320

321

322

323

324

325

To verify that the CESM2-LE is a viable tool for the analysis of large-scale convective environments, the fifth-generation global climate reanalysis (ERA5; Hersbach et al., 2020) from the European Centre for Medium-Range Forecast (ECMWF) was used for model validation. Previous studies have found ERA5 to be reliable in capturing the spatiotemporal climatology of convective environments (Taszarek et al., 2021). In particular, F. Li et al. (2020) conducted a climatological analysis of severe local storm environments over North America using ERA5 compared to CAM6 simulations of the historical period. They confirmed the validity of ERA5 against 69 radiosonde observations over the CONUS region with twice daily raw soundings and further confirmed the fidelity of CAM6 against ERA5. This is important because, relative to its predecessor CAM5 (Neale & Gettelman, 2012), CAM6 underwent significant modifications to the physical parameterization suite. Updates to the Zhang and McFarlane (1995) deep convection and orographic drag parameterizations were implemented into CAM6, along with the two-moment prognostic cloud microphysics from Gettelman and Morrison (2015). Additionally, the Cloud Layers Unified by Binormals (CLUBB; Golaz et al., 2002) replaced schemes for cloud macrophysics, boundary layer turbulence, and shallow convection previously used in CAM5, all of which are key parameterizations for modeling convection.

The MAMJ CAPES06 climatology from ERA5 (left) and the ensemble-mean climatology from CESM2-LE (right) is shown in Fig. 2 over the CONUS region. There is strong agreement between the CESM2-LE and ERA5 during 1980-2019, indicating that the model successfully captures the mean spatial characteristics of CAPES06 over the past 40 years. Although not shown, similarly strong agreement is found between ERA5 and CESM2-LE for the climatologies of the other convective indices (CAPE, CIN, and S06).

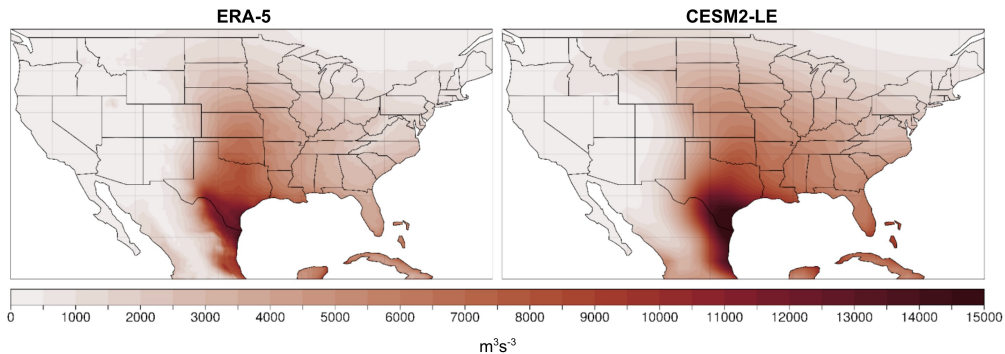


Figure 2. MAMJ CAPES06 (m^3s^{-3}) climatology for ERA5 reanalysis (left) and the CESM2-LE ensemble-mean (right) for the 1980-2019 period.

326

327

328

329

330

331

332

333

334

335

To further examine the fidelity of the CESM2-LE, we investigated the relationship between CAPES06 and ENSO, the largest driver of interannual changes in weather and climate over much of the globe (Ropelewski & Halpert, 1986; Dai et al., 1997; Allen et al., 2015; Dai & Wigley, 2000). The regression of boreal spring CAPES06 from ERA5 onto the observed Niño3.4 index over 1980-2019 is shown in Fig. 3 on the left, compared to the same quantity from the CESM2-LE over 1870-2019 on the right. Notably, CESM2-LE captures the main changes in CAPES06 associated with ENSO, including large-scale decreases in CAPES06 over the eastern CONUS during El Niño, with increases over the western CONUS. Since this study utilizes a large ensemble, many more El Niño events are sampled from the CESM2-LE data than from ERA5, resulting in more coherent spa-

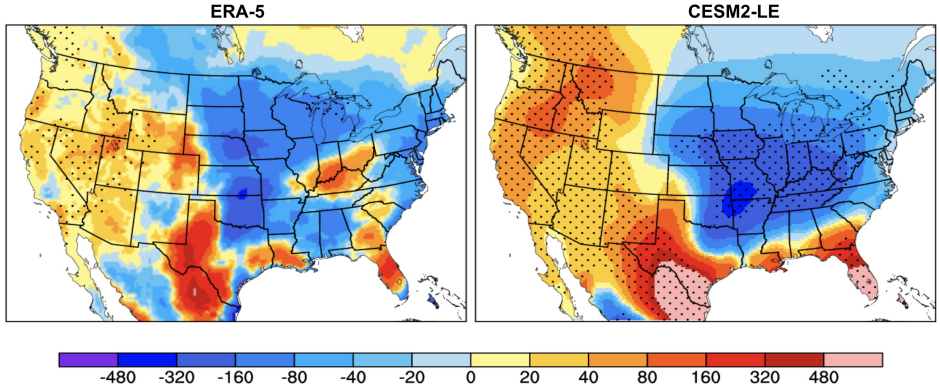


Figure 3. Regression of CAPES06 onto the ENSO index for one standard deviation over the MAMJ season from ERA5 reanalysis (1980-2019; left) and the CESM2-LE (1870-2019; right). Stippling on ERA5 shows the 95% statistical significance based on the Students T-test. Stippling on CESM2-LE indicates where 45 of the 50 members have the same sign.

336 tial patterns. This relationship is consistent with other studies that have investigated
 337 the role of ENSO on severe weather outbreaks over the U.S. during the March-May season
 338 (e.g., Lee et al., 2013; Allen et al., 2015). The results in this section, combined with
 339 the findings of earlier studies (e.g., F. Li et al., 2020), give us confidence in using the CESM2-
 340 LE to examine past and future changes in convective environments over the CONUS,
 341 as well as the variations driven by internal modes of climate variability (e.g., Capotondi
 342 et al., 2020; Rodgers et al., 2021).

343 3 Results

344 3.1 Ensemble Mean (Forced Changes)

345 The historical and future time evolution of the selected convective indices from 1870-
 346 2100 for the boreal spring season averaged over the eastern CONUS (Fig. 1) are shown
 347 in Fig. 4. The time series are expressed as seasonal anomalies relative to the 30-year base
 348 period 1971-2000. The forced component of climate change is given by the ensemble-mean
 349 of the CESM2-LE, represented by the solid black line, and the time evolution of indi-
 350 vidual ensemble members are depicted by the light gray lines. While considerable run-
 351 to-run, interannual and decadal variability is evident in individual ensemble members,
 352 the forced response in convective indices show minimal change from 1870 until about 1990,
 353 deviating little from the 30-year baseline climatologies. However, right around the year
 354 2000, forced changes in convective environments become apparent and exhibit clear de-
 355 partures from the historical climatological values throughout the current century. For
 356 instance, ensemble-mean values of CAPE steadily increase throughout the 21st century,
 357 exceeding the historical climatological values by nearly 400 Jkg^{-1} by 2100 (Fig. 4a), while
 358 the forced change in S06 becomes more negative. Specifically, anomalies in S06 reach ap-
 359 proximately -2 ms^{-1} by 2075, then remain near that level through the remainder of the
 360 century (Fig. 4b).

361 The time evolution of CAPES06 (Fig. 4c) exhibits behavior similar to that of CAPE,
 362 with an almost linear increase from 2000 of $\sim 3500 \text{ m}^3\text{s}^{-3}$ above the historical climatol-
 363 ogy by 2100. The time history of CIN also shows little deviation until this century, when
 364 it exhibits a steady decrease in magnitude to approximately -18 Jkg^{-1} by 2100 (Fig. 4d).
 365 These results show that changes in convective environments due to anthropogenic forc-
 366 ing through the end of this century are prominent and robust in CESM2-LE, as they are

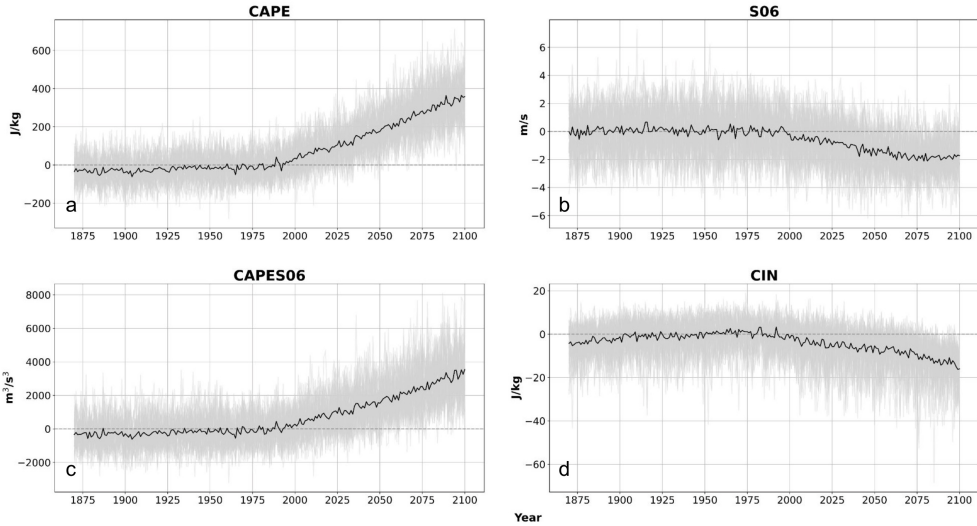


Figure 4. Time series of convective indices from 1870-2100 for (a.) CAPE (Jkg^{-1}), (b.) S06 (ms^{-1}), (c.) CAPES06 (m^3s^{-3}), and (d.) CIN (Jkg^{-1}) over the eastern CONUS region. The 50-member ensemble-mean (black) is superimposed on individual members (light grey).

367 reflected in nearly all of the 50 members of the ensemble (light grey lines in Fig. 4). Few
 368 previous studies have been able to estimate the continuous-time evolution of changes in
 369 these convective indices. One example is Diffenbaugh et al. (2013), who leveraged the
 370 CMIP5 to take regional averages over eastern CONUS for CAPE, S06, and NDSEV from
 371 1960-2100 using RCP8.5. Furthermore, Trapp et al. (2009) used a five-member ensemble
 372 from the Community Climate System Model version 3 (CCSM3) to take various regional
 373 averages in areas over the CONUS that frequently encounter severe weather, including
 374 the southeast, Midwest, and the southern and northern Great Plains. This was done
 375 for the same indices as Diffenbaugh et al. (2013) but from 1950-2100. In general,
 376 the trends and magnitudes of the changes in these indices are in agreement with the changes
 377 expressed in Fig. 4, especially over the southern Plains and southeast CONUS, as seen
 378 in Trapp et al. (2009). The principal point is that convective environments over the eastern
 379 CONUS during the boreal spring are likely to undergo substantial departures from the
 380 historical record over this century (Fig. 4), moving toward higher convective energy,
 381 more stability, and less kinematic support for the production of hazards associated with
 382 severe weather.

383 To evaluate the spatial character of these changes over the CONUS, epoch differences
 384 for future 30-year periods relative to the 1971-2000 baseline climatology are shown
 385 in Fig. 5. By 2100, the CESM2-LE projects spatially coherent forced changes in convective
 386 environments relevant to the frequency and intensity of severe weather. Over the
 387 next few decades (2021-2050), increases in CAPE are largest near the Gulf coast and are
 388 positive across the entire CONUS (Fig. 5a). These changes in CAPE are projected to
 389 strengthen throughout the rest of this century, primarily over the eastern CONUS and
 390 southern Plains (Trapp et al., 2007; Diffenbaugh et al., 2013; Seeley & Romps, 2015; Hoogewind
 391 et al., 2017; K. L. Rasmussen et al., 2017; Chen et al., 2020; Lepore et al., 2021). As CAPE
 392 is related to the maximum potential updraft within a thunderstorm by $w_{max} = \sqrt{2CAPE}$
 393 (Holton & Hakim, 2013), projections of higher CAPE imply that, on average, future storms
 394 will have stronger updrafts, resulting in deeper, more explosive convection than storms
 395 during the reference period (1971-2000). Additionally, it was shown by Dougherty and
 396 Rasmussen (2021) that updraft intensities increased in flood-producing storms in CONUS

397 simulations, further supporting the hypothesis that increasing CAPE results in an in-
 398 creased risk for severe weather. The spatial patterns in these changes also highlight the
 399 continued influence of the GPLLJ advecting warm, moist air into the Plains and east
 400 of the Rocky Mountains (e.g., Carlson et al., 1983).

401 Epoch differences in boreal spring wind shear reveal a large and spatially coherent
 402 east-west swath of decreasing S06 over the entirety of the CONUS, increasing in mag-
 403 nitude with time in Fig. 5b (Trapp et al., 2007, 2009; Diffenbaugh et al., 2013; Hoogewind
 404 et al., 2017; Lepore et al., 2021; Ting et al., 2019). The greatest changes appear in the
 405 northeast, with smaller decreases over the southern CONUS. Sufficient shear is impera-
 406 tive to the internal dynamics of a thunderstorm since it promotes vertical storm-scale
 407 rotation and assists in sustaining the updraft (Weisman & Rotunno, 2000; Trapp et al.,
 408 2007), which are important ingredients for tornadogenesis, large hail formation, and dam-
 409 aging outflow winds at the surface. Additionally, storm environments characterized by
 410 strong vertical wind shear are more likely to be organized, last longer, and become self-
 411 sustaining systems (e.g., Lilly, 1979; Rotunno, 1981; Klemp, 1987; Weisman & Rotunno,
 412 2000). For these reasons, decreases in shear with time indicate that increasingly fewer
 413 thunderstorms will have the support necessary for the most hazardous and severe storms
 414 to form, including organized mesoscale convective systems (MCS).

415 To further diagnose the projected changes in S06, the changes of zonal and merid-
 416 ional winds near the surface and at 6-km were also analyzed. Future projections of sur-
 417 face winds do not reveal spatially coherent changes over the next century, but the zonal
 418 winds aloft indicate substantial departures from the historical record. In particular, nearly
 419 all of the CESM2-LE members project decreases in upper-level westerly winds over the
 420 CONUS during the boreal spring season that increase in magnitude with time. The causal
 421 mechanisms of these zonal wind changes are being explored further, but preliminary re-
 422 sults suggest a connection to projected future changes in tropical rainfall patterns (not
 423 shown).

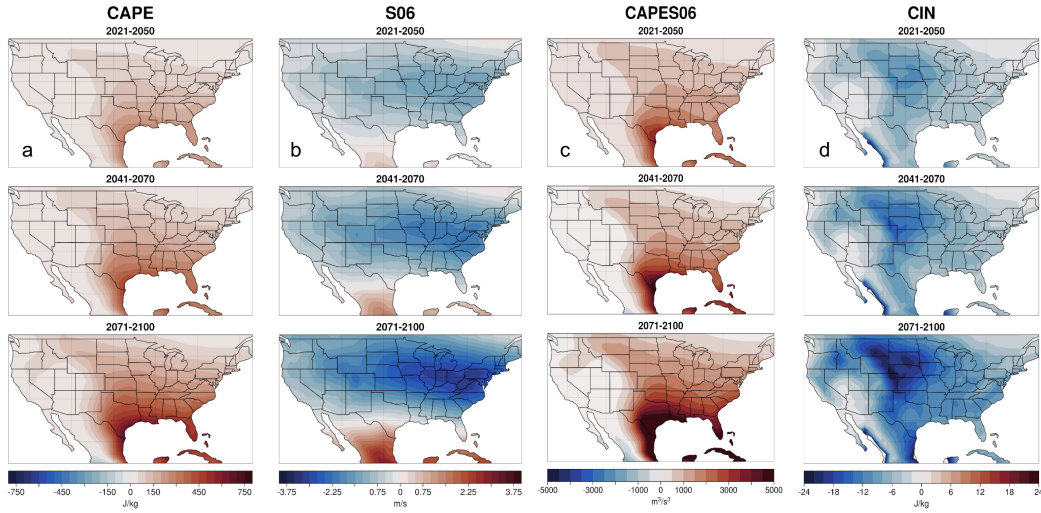


Figure 5. Epoch differences from the 1971-2000 baseline period for early (2021-2050), mid (2041-2070), and end-of-century (2071-2100) convective indices during MAMJ for (a.) CAPE (Jkg^{-1}) (b.) S06 (ms^{-1}) (c.) CAPES06 (m^3s^{-3}) and (d.) CIN (Jkg^{-1})

424 The projected spatial characteristics of changes in CAPES06 (Fig. 5c) are simi-
 425 lar to those highlighted by (Seeley & Romps, 2015), who leveraged four climate mod-

426 els, archived from CMIP5 and forced with two different emission scenarios, to compare
 427 the end-of-century projections of CAPES06 over the U.S. Overall, their findings, as well
 428 as ours, show spatial patterns of boreal spring CAPES06 that are dominated by the changes
 429 in CAPE (Fig. 5a), characterized by a coherent increase with time over the eastern CONUS.
 430 Although the decreases in S06 suggest that there would be less support for storm organ-
 431 ization and dynamics, some studies speculate that the large-scale increases in CAPE will
 432 make up for the diminishing S06 (Trapp et al., 2007, 2009). The main point is that CAPES06
 433 is expected to undergo substantial increases by the end of this century, suggesting con-
 434 vective environments over the southeastern U.S. will be supportive of a higher ratio of
 435 significant severe versus non-severe storms.

436 However, this hypothesis does not take into account the increasing magnitude of
 437 CIN that represents the negative buoyancy that parcels need to overcome in order to re-
 438 alize their CAPE (K. L. Rasmussen et al., 2017). Despite enhanced CAPE values in a
 439 future climate, weak to moderate storms may be less frequent due to enhanced stabil-
 440 ity (i.e. CIN) that requires more lifting or heating to overcome. Changes in the forced
 441 component of CIN projected by the CESM2-LE are characterized by decreases over the
 442 central and northern Great Plains that increase in magnitude throughout this century,
 443 reaching approximately -18 Jkg^{-1} by 2100 (Fig. 5d). Such changes are indicative of a
 444 more stable or “capped” atmosphere. If strong enough ($\text{CIN} < -200 \text{ Jkg}^{-1}$), this stabil-
 445 ity could potentially inhibit convection completely. On the other hand, there is the possi-
 446 bility that there is moderate CIN ($-50 \text{ Jkg}^{-1} > \text{CIN} > -200 \text{ Jkg}^{-1}$), allowing for an ac-
 447 cumulation of CAPE that once released, could produce explosive convection. Globally,
 448 this is commonly observed in convective environments in the vicinity of large mountain
 449 ranges such as the Rockies and the Andes, as discussed in the introduction (Zipser et
 450 al., 2006; K. L. Rasmussen & Houze, 2011; K. L. Rasmussen et al., 2014; K. L. Rasmussen
 451 & Houze, 2016). The juxtaposition of the terrain-induced mid-level capping inversion
 452 with the warm, moist air allows for the modulation of CAPE by CIN until convective
 453 initiation occurs and intense convection is then able to develop. It is also evident in the
 454 spatial patterns (Fig. 5) that by the end of the century, the areas of maximum stabil-
 455 ity are not collocated with the areas of maximum convective energy. Therefore, since CIN
 456 is minimized over the Great Plains, while CAPE is maximized over the eastern U.S., the
 457 future frequency of convection in the Great Plains is, on average, likely to be less than
 458 the current climate but still vigorous due to increased stability, while convective frequency
 459 over the eastern U.S. is likely to be slightly less reduced, but more intense when it does
 460 occur as a result of the increased and accumulated CAPE. Overall, these changes are in
 461 agreement with previous studies using both Earth system models (Hoogewind et al., 2017;
 462 Lepore et al., 2021) and dynamical downscaling or a pseudo-global warming approach,
 463 such as K. L. Rasmussen et al. (2017) and Chen et al. (2020), projecting coherent increases
 464 in the magnitude of CIN over the central and southern Great Plains by 2100 (Fig. 5d).

465 Following the analyses of Brooks et al. (2003), Trapp et al. (2007), and Gensini and
 466 Ashley (2011), the number of days favorable for the formation of severe weather is de-
 467 termined by computing NDSEV. Early-century (2021-2050) changes from the baseline
 468 climatology show an increase in boreal spring NDSEV that is especially pronounced over
 469 the eastern half of the CONUS, with the largest values over the southeastern U.S. (Fig.
 470 6). Increases in NDSEV continue throughout the rest of this century, yielding values more
 471 than double the historical climatology, and largely reflecting spatial patterns evident in
 472 CAPE (Fig. 5a). These findings are further evidence that, by 2100, eastern CONUS will
 473 likely experience an increase in severe storm activity, despite the robust decrease in pro-
 474 jections of S06, especially since the end of century magnitudes of wind shear are still larger
 475 than the severe weather threshold (5 ms^{-1}) (Brooks et al., 2003; Trapp et al., 2007, 2009;
 476 Diffenbaugh et al., 2013; Hoogewind et al., 2017). While the spatial patterns of change
 477 in NDSEV are in broad agreement with previous studies, the magnitude of changes ex-
 478 pected by the end of the century are larger than the aforementioned studies. A detailed
 479 explanation for these differences is beyond the scope of this paper, but it should be noted

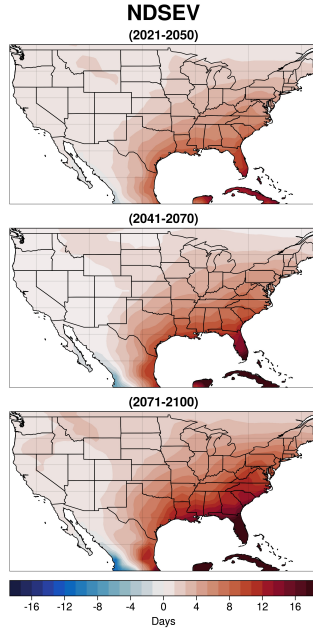


Figure 6. Same as Fig. 5, except for NDSEV (Days).

480 that other studies used slightly different definitions of NDSEV as well as different mod-
 481 els with various forcing scenarios, all of which likely contribute to deviations from the
 482 results shown in Fig. 6.

483 As expressed, the results in this section for CAPE, CIN, S06, and CAPES06 are
 484 all in general agreement with previous literature. What makes this work unique is that
 485 we have been able to show a robust, multi-century estimate of the large-scale convective
 486 environment over the eastern U.S. by using a 50-member ensemble, providing more cer-
 487 tainty in the changes of the forced response due to anthropogenic climate change as sim-
 488 ulated by the CESM2.

489 3.2 Internal Variability

490 Previous studies have primarily focused on changes in convective environments due
 491 to anthropogenic climate change (i.e., the forced response). However, the large ensem-
 492 ble approach provides a novel opportunity to investigate the effect of internal (or unforced)
 493 climate variability and how it might modify the forced response, where all 50 ensemble
 494 members represent an equally possible path to reality. To illustrate the range of possi-
 495 ble outcomes, the simple metric of linear trends for each of the convective indices over
 496 the next 30 years (2021-2050) is considered. Histograms of the ensemble members are
 497 shown in Fig. 7. Changes through 2050 are analyzed because uncertainty due to inter-
 498 nal climate variability is most significant over the next several decades relative to the
 499 forced signal (Hawkins & Sutton, 2009; Deser, 2020).

500 Even in the presence of significant internal variability, 30-year trends of boreal spring
 501 CAPE over the eastern CONUS are positive for all 50 ensemble members (Fig. 7a), but
 502 they exhibit considerable spread. Trends out to 2050 range from near zero to $\sim 68 \text{ Jkg}^{-1}\text{decade}^{-1}$,
 503 while two-thirds of the ensemble members have CAPE trends between 20 and $40 \text{ Jkg}^{-1}\text{decade}^{-1}$.
 504 Similarly, trends in S06 are mostly of the same sign, with 46 of the 50 ensemble mem-
 505 bers exhibiting negative trends with a minimum of $-0.85 \text{ ms}^{-1}\text{decade}^{-1}$ projected by four
 506 members. These results show that the sign of the response of CAPE and S06 to anthro-

507 pogenic forcing (Fig. 4a, b) is robust across nearly all of the CESM2-LE members, but
 508 that the magnitude of the forced response is likely to be considerably moderated by in-
 509 ternal climate variability over the coming decades (Fig. 7a, b). It follows that boreal spring
 510 trends in CAPES06 over the coming decades are positive for nearly all ensemble mem-
 511 bers (Fig. 7c), with 80% of the members exhibiting trends between 100 and 500 $\text{m}^3\text{s}^{-3}\text{decade}^{-1}$.
 512 In contrast, the signs of 30-year trends in boreal spring CIN over the eastern CONUS
 513 are more mixed (Fig. 7d). Twenty-one of the ensemble members exhibit positive trends,
 514 while the other 29 exhibit negative trends down to $-4.25 \text{ Jkg}^{-1}\text{decade}^{-1}$ (Fig. 7d). While
 515 Fig. 4d illustrates a forced decrease in CIN magnitudes by the end of the century, the
 516 robustness of the sign of the change is less certain due to internal climate variability when
 517 averaged over the eastern CONUS (Fig. 7d).

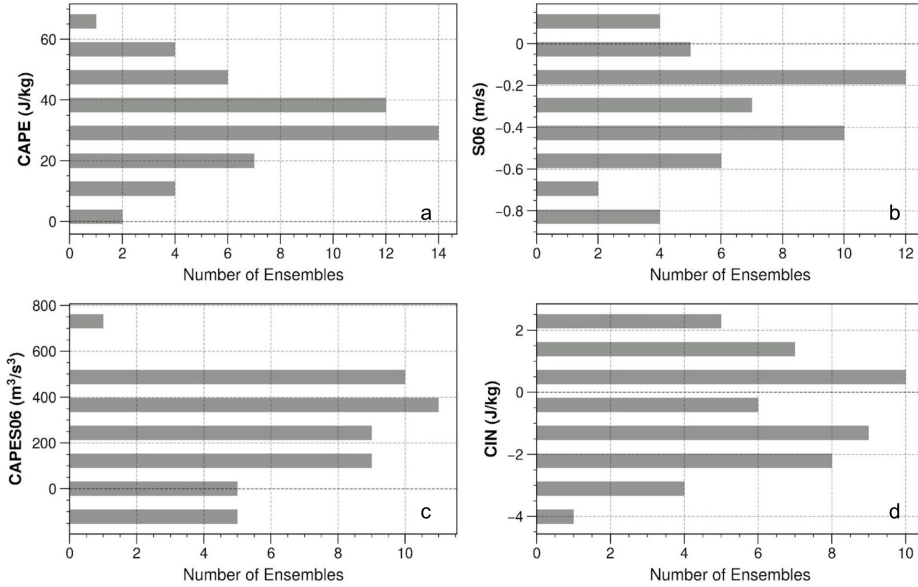


Figure 7. Histograms for 50-member ensemble simulations illustrating the spread of linear trends per decade for the 2021-2050 period during the months March - June for (a.) CAPE ($\text{Jkg}^{-1}\text{decade}^{-1}$) (b.) S06 ($\text{ms}^{-1}\text{decade}^{-1}$) (c.) CAPES06 ($\text{m}^3\text{s}^{-3}\text{decade}^{-1}$) (d.) CIN ($\text{Jkg}^{-1}\text{decade}^{-1}$). Linear trends were calculated using ordinary least squares linear regression and spatial averages were taken over the eastern CONUS region highlighted in Figure 1.

518 To further illustrate the dominant role that internal climate variability is likely to
 519 play over the next several decades, we examine spatial patterns of change by selecting
 520 the ensemble members with the largest and smallest trends in area-averaged convective
 521 indices over the eastern CONUS during the boreal spring seen in Fig. 7. CAPES06 is
 522 discussed since it considers two of the most important elements necessary for severe weather:
 523 the thermodynamic energy and kinematic support (Fig. 8).

524 Ensemble member 25 exhibits the most negative (minimum) CAPES06 trend (-182
 525 $\text{Jkg}^{-1}\text{decade}^{-1}$) when averaged over the eastern CONUS, while ensemble member 23 has
 526 the largest trend ($791 \text{ Jkg}^{-1}\text{decade}^{-1}$) (Fig. 7c). The spatial patterns of the linear decadal
 527 trends in CAPES06 for these two simulations are shown in Fig. (8a, d), respectively. By
 528 removing the forced trend (ensemble-mean) from each of these individual ensemble mem-
 529 bers (Fig. 8b, e), the changes in CAPES06 over the next several decades due purely to
 530 internal variability are revealed (Fig. 8c, f). In general, the signals of internal climate

531 variability are spatially coherent and are of a larger magnitude over the next several decades
 532 than the forced trends. In ensemble member 25, internal climate variability counteracts
 533 the forced, positive change in CAPES06 over much of the southeastern U.S. (Fig. 8c),
 534 resulting in an overall negative trend over much of the region (Fig. 8a). Conversely, in
 535 ensemble member 23, internal climate variability (Fig. 8f) augments the forced signal
 536 and produces a very strong increase through 2050, especially over parts of Texas and the
 537 southern Great Plains (Fig. 8d). These two ensemble members were subjectively selected
 538 to most dramatically illustrate the role of internal climate variability in modulating the
 539 forced response in CAPES06, but a similar approach can be taken with the other ensem-
 540 ble members in Fig. 7 to illustrate the large-scale, coherent spatial patterns of internal
 541 variability that significantly modify the forced trend.

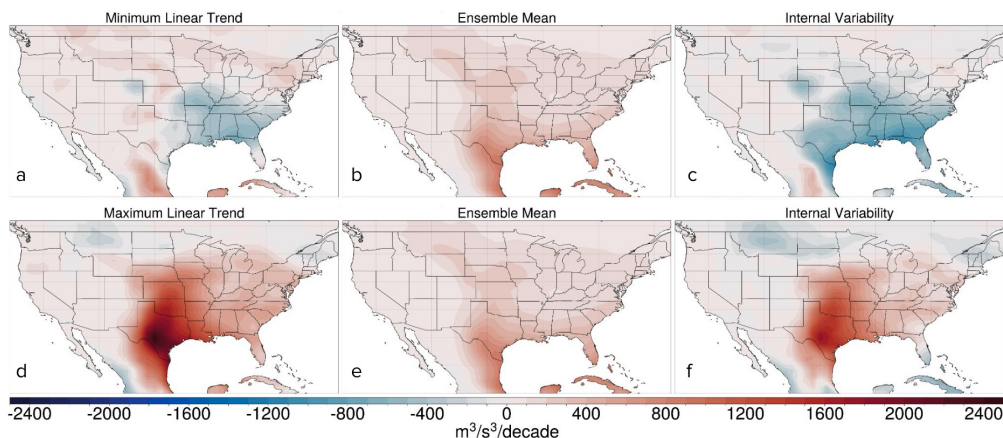


Figure 8. Linear decadal trends for 2021-2050 over the eastern CONUS for the ensemble numbers 25 (top row) and 23 (bottom row) for the full (left; a, d), forced (middle; b, e), and internal (right; c, f) components of MAMJ CAPES06 ($\text{m}^3\text{s}^{-3}\text{decade}^{-1}$).

542 Similarly, the dominant role of internal variability in affecting NDSEV is illustrated
 543 in Fig. 9. On average, over the next several decades (2021-2050), anthropogenic climate
 544 change is likely to increase the number of days in boreal spring with convective environ-
 545 ments favorable for the development of severe weather over most of the CONUS, with
 546 the largest increases over the southeastern U.S. (Fig. 9b, 9e). However, as shown by en-
 547 semble member 41 (Fig. 9a), a plausible outcome by 2050 is that internal climate vari-
 548 ability could substantially reduce the number of days favorable for severe weather (Fig.
 549 9c). Conversely, ensemble member 23 shows that internal climate variability (Fig. 9f)
 550 could augment the increases from climate change, resulting in a large increase in ND-
 551 SEV by 2050 (Fig. 9d). While internal fluctuations may be considered to be inherently
 552 chaotic and random, they are a product of the large-scale dynamics and thus, are spa-
 553 tially coherent with relatively large magnitudes (Fig. 8, 9). Further examining the cir-
 554 culation anomalies that drive such internal variations in these convective parameters is
 555 the subject of future work. A key point is that when considering future projections of
 556 greenhouse-gas forced changes in severe weather environments, the extent to which they
 557 will be modulated by internal variability is important to consider.

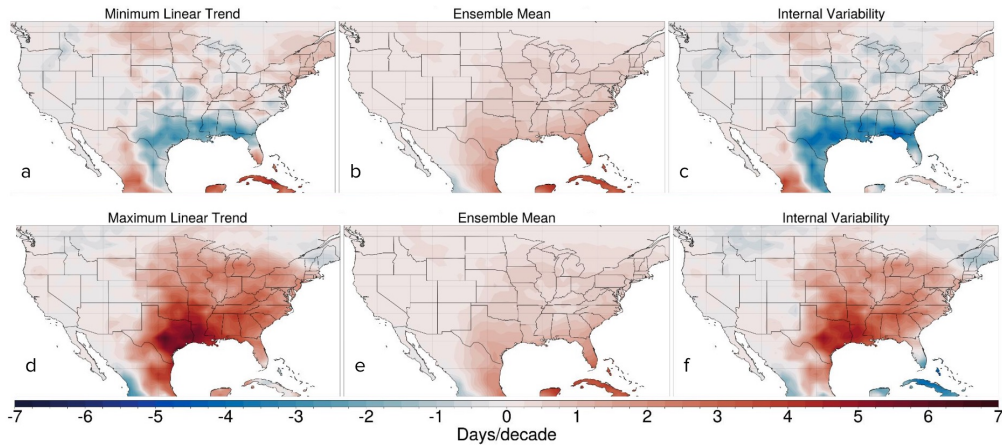


Figure 9. Linear decadal trends for 2021-2050 over the eastern CONUS for the ensemble numbers 41 (top row) and 23 (bottom row) for the full (left; a, d), forced (middle; b, e), and internal (right; c, f) components of MAMJ NDSEV (Daysdecade^{-1}).

558 In addition to employing covariate proxies, epoch bivariate distribution plots, or
 559 two-dimensional histograms, were created to examine the future phase spaces (i.e., con-
 560 vective frequency and intensity) of various convective indices, due to both forced and in-
 561 ternal variability, to gain more insight into changes in the convective mode. As mentioned
 562 earlier, K. L. Rasmussen et al. (2017) used dynamical downscaling to produce convection-
 563 permitting regional climate model projections of end-of-century (2071-2100) May-June
 564 CAPE and CIN over the Midwest to examine changes in the thermodynamic environ-
 565 ment. By producing a two-dimensional histogram, they found that by the end of the cen-
 566 tury, convective environments are increasingly characterized by higher average CAPE
 567 ($\sim 400 \text{ Jkg}^{-1}$) and lower average (or increased) CIN ($\sim -80 \text{ Jkg}^{-1}$) indicative of more
 568 vigorous convective storms but a stronger capping inversion. We have taken a similar
 569 approach using the CESM2-LE to illustrate changes in both the forced and internal com-
 570 ponents of the convective indices over time. The bivariate distributions of the histor-
 571 ical climatology (1971-2000, blue) and future 30-year periods (2021-2050, orange; and 2071-
 572 2100, green) are shown in Fig. 10. Individual, or marginal, distributions are displayed
 573 on the opposite axis for each index, helping to highlight the range due to internal vari-
 574 ability, and how it changes through the century. While the shape of the distribution gives
 575 some insight into the range of internal variability, the shifts in the CAPE versus CIN pat-
 576 tern as a whole are due to the changes over time in the forced response.

577 For the late 20th century (blue), the distribution in Fig. 10a has the highest den-
 578 sity of ensemble members around CAPE values of 440 Jkg^{-1} and CIN values around -
 579 29 Jkg^{-1} . Over the next several decades (orange), the distribution exhibits an overall
 580 shift toward the bottom right of the diagram with relatively higher CAPE (560 Jkg^{-1})
 581 and relatively lower, or increased magnitudes, of CIN (-36 Jkg^{-1}). By the end of the 21st
 582 century (green), the CAPE versus CIN distribution has shifted to even higher CAPE and
 583 lower CIN, with average magnitudes of $\sim 745 \text{ Jkg}^{-1}$ and -40 Jkg^{-1} , respectively (Fig.
 584 10a). In Fig. 10a, the shape of the end-of-century epoch (green) indicates that the fu-
 585 ture projections of CAPE could be anywhere from approximately 500 to 1050 Jkg^{-1} by
 586 the end of the century. Conversely, even with an ensemble mode of -40 Jkg^{-1} , the range
 587 of future projections for CIN due to the internal variability could fall anywhere between
 588 -26 and -70 Jkg^{-1} (Fig. 10a). Thus, even though a wide range of plausible outcomes ex-
 589 ist for both CAPE and CIN due to the role of internal variability, a majority of the en-
 590 semble members suggest future environments over the southeastern CONUS will be com-

591 posed of higher CAPE and increased magnitudes of CIN compared to the present-day
 592 climate (Diffenbaugh et al., 2013; K. L. Rasmussen et al., 2017; Lepore et al., 2021). The
 593 balance between these two thermodynamic indices is key to determining future convective
 594 modes and frequency (Diffenbaugh et al., 2013; K. L. Rasmussen et al., 2017; Chen
 595 et al., 2020; Lepore et al., 2021).

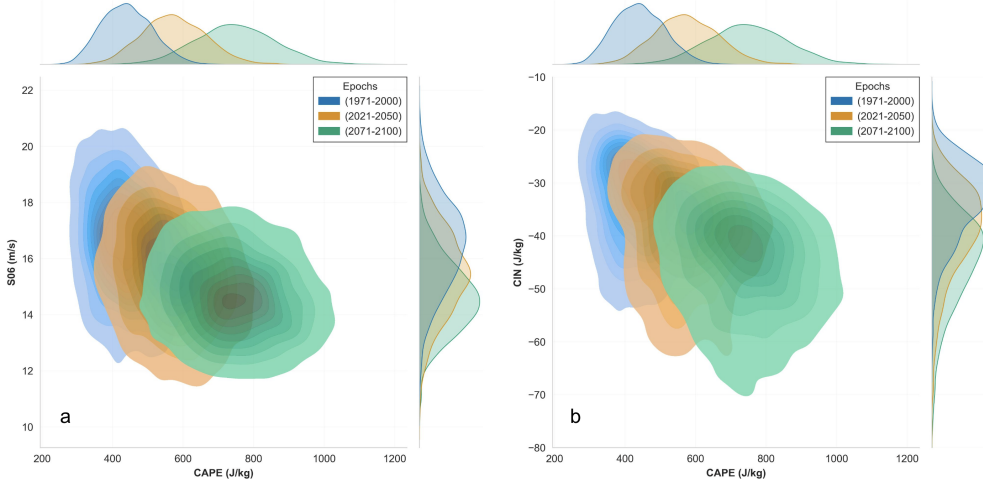


Figure 10. Bivariate distributions over eastern CONUS for MAMJ (a.) CAPE (Jkg^{-1}) vs. CIN (Jkg^{-1}) and (b.) CAPE (Jkg^{-1}) vs. S06 (ms^{-1}) for various epochs: 1971-2000 in blue, 2021-2050 in orange, and 2071-2100 in green. Marginal distributions for each index and period are shown on the opposite axis.

596 The same analysis can be done for the CAPE and vertical wind shear phase space
 597 (Fig. 10b), which is key for storm type and organization. Overall, the phase space of these
 598 two indices shifts from relatively moderate CAPE and high S06 to higher CAPE and lower
 599 S06 (Trapp et al., 2007; Diffenbaugh et al., 2013; Hoogewind et al., 2017; Lepore et al.,
 600 2021). The CAPE distributions are the same as Fig. 10a, but the distribution in bulk
 601 vertical wind shear follows a decreasing trend throughout the century, with an ensemble
 602 mode of approximately 14.5 ms^{-1} by 2100 (Fig. 10b, green). It is also clear that, from
 603 the historical climatology to the end of the century, the shapes of the epochs evolve from
 604 long and narrow to a more circular shape. In other words, the uncertainty in S06 changes
 605 due to internal variability is likely to decrease as the century progresses, whereas the un-
 606 certainty in changes to CAPE is likely to increase. Previously, Brooks et al. (2003) an-
 607 alyzed soundings from reanalysis data that were associated with severe thunderstorms
 608 in the U.S. from 1997-1999. These soundings were further classified as little severe, sig-
 609 nificant severe, and significant tornadoes. Their two-dimensional histogram of CAPE and
 610 S06 indicated the most severe storms were characterized by high CAPE and high wind
 611 shear (i.e., the top right of Fig. 10b). Further, the storms that were classified as sig-
 612 nificant tornadoes had S06 greater than 10 ms^{-1} , and storms that were classified as sig-
 613 nificant severe exhibited S06 greater than 5 ms^{-1} . The distribution for significant severe
 614 storms existed over the high CAPE region ($100\text{-}5000 \text{ Jkg}^{-1}$), but significant tornadoes
 615 exhibited values across the full range of CAPE distributions.

616 Comparing our results to the storm classifications in Brooks et al. (2003) and other
 617 studies (E. N. Rasmussen & Blanchard, 1998; Brooks, 2009), the projected increases in
 618 end-of-century CAPE will be more than sufficient to support significant severe storms
 619 and tornadoes. Although, while S06 is projected to decrease, even in the presence of in-

620 ternal variability, the absolute magnitudes of wind shear (Fig. 10b) remain above the
 621 threshold to produce significant severe weather, but may not be as supportive of the most
 622 intense types of severe weather (e.g. tornadoes or derechos). The implication of higher
 623 CAPE and lower S06 is that when future storms do occur, there is a smaller chance that
 624 they will have the necessary dynamical support and organization to produce the most
 625 intense severe weather compared to the current climate, paralleling past research (Difffenbaugh
 626 et al., 2013; Lepore et al., 2021).

627 4 Discussion and Conclusion

628 An important goal of this study was to better understand how severe and hazardous
 629 weather is likely to change in a warmer, future climate. While the spatiotemporal scales
 630 on which severe storms form are smaller than can be explicitly resolved by relatively coarse
 631 resolution models such as the CESM2, such models can be leveraged to instead exam-
 632 ine the evolution of the large-scale convective environments in which the storms develop.
 633 Further, by using a large ensemble of climate model simulations as we have done with
 634 the CESM2-LE, it is possible to not only identify and examine anthropogenically-forced
 635 changes in convective environments over time but also how the forced changes are likely
 636 to be altered by internal climate variability. This latter aspect, to our knowledge, has
 637 yet to be robustly documented. An increased understanding of the range of plausible,
 638 future convective environments can enhance our capability to better project the nature
 639 of severe weather in the future, and perhaps increase resilience to these hazards.

640 Our study is novel in that we have examined the continuous-time evolution of var-
 641 ious convective indices from 1870-2100 over the CONUS using a 50-member ensemble
 642 from a well-documented and understood Earth system model. By using a large ensem-
 643 ble from a single model, we were able to obtain a robust estimate of the forced response.
 644 Our results are in agreement with previous studies that anthropogenic climate change
 645 will likely drive future convective environments over the eastern U.S. toward less frequent,
 646 but more intense and deep convection. Additionally, there will also be less kinematic sup-
 647 port, which means less support for the organization of supercells and other multi-cellular
 648 convective storm modes capable of delivering the most extreme severe weather risks.

649 By taking advantage of a large ensemble approach, this study was further able to
 650 robustly investigate the effect of internal climate variability on large-scale convective en-
 651 vironments, rather than just the forced response as most previous studies have done. While
 652 we have shown that the end-of-century changes in convective environments due to the
 653 forced response are spatially coherent and robust, we have also demonstrated how these
 654 changes can be substantially modulated by internal variability. The latter has spatial
 655 coherency and thus can either significantly enhance or suppress the forced changes.

656 Examining the convective proxies and the bivariate distributions of the selected in-
 657 dices, it is likely that future environments will be characterized by higher CAPE, moderate-
 658 high magnitudes of CIN, and lower S06, which is in general agreement with previous lit-
 659 erature. Our results thus suggest that there will be an increase in frequency in the less
 660 severe convective modes such as multi-cellular and ordinary thunderstorms. The actual
 661 time evolution of these quantities will, of course, not only be influenced by forced climate
 662 change, but also by internal variability. While it is not possible to make a determinis-
 663 tic prediction of how actual convective environments over the CONUS will evolve through-
 664 out the rest of this century, our study has helped to quantify the range of uncertainty
 665 and plausible scenarios.

666 Our conclusions depend on the assumption that the CESM2-LE is capable of ac-
 667 curately simulating the future, even though it performs well in simulating past convective
 668 environments (e.g., Figs. 2, 3). Our results are also dependent on the future forc-
 669 ing scenario (SSP3-7.0) used to produce the CESM2-LE.

This study is the first to exploit the CESM2-LE to examine changes in convective parameters. Plans for future work include more comprehensive regional analyses, especially since some regions are less influenced by internal variability than others (Deser et al., 2012b), and in this study, averages have been taken over a very large spatial domain (Fig. 1). Also, given the prominent and coherent role of internal variability over the southeastern U.S., further analysis is necessary to examine the large-scale circulation changes that drive internal variations in the convective indices, and if those circulation changes are connected to large-scale coupled modes of climate variability. If so, it will be important to determine the level of predictability associated with internal variability. Finally, similar analyses for other seasons, as well as other regions of the world where convective activity is pronounced, such as over Argentina on the lee-side of the Andes (e.g., Zipser et al., 2006; K. L. Rasmussen & Houze, 2011; K. L. Rasmussen et al., 2014; Mulholland et al., 2018; Nesbitt et al., 2021) are underway. A better understanding of the possible future evolution and variability in large-scale convective environments is critical for understanding future changes in severe weather hazards and in particular, how we choose to adapt to these hazards.

Open Research Section

The first 50 ensemble members from The Community Earth System Model Version 2-Large Ensemble data (CESM2-LE; Danabasoglu et al., 2020; Rodgers et al., 2021) used for this study can be found and downloaded publicly online at <https://doi.org/10.26024/kgmp-c556>. Data from the Fifth-Generation Global Climate Reanalysis (ERA5; Hersbach et al., 2020) can also be found and downloaded publicly online at <https://doi.org/10.5065/BH6N-5N20>.

Acknowledgments

We would like to acknowledge the CESM2 Large Ensemble Community Project and supercomputing resources provided by the IBS Center for Climate Physics in South Korea. In addition, we would also like to acknowledge Dan Chavas of Purdue University for preliminary conversations regarding this project, as well as for providing us with the calculated ERA5 convective parameters used in this study. Thank you to the listed co-authors for their support and guidance in completing this project as well as to the Department of Atmospheric Science and the Walter Scott, Jr. College of Engineering at Colorado State University.

References

- Allen, J. T., Tippet, M. K., & Sobel, A. H. (2015). Influence of the El Niño/Southern Oscillation on tornado and hail frequency in the United States. *Nature Geoscience*, *8*(4), 278–283. doi: 10.1038/ngeo2385
- Brooks, H. E. (2009). Proximity soundings for severe convection for Europe and the United States from reanalysis data. *Atmospheric Research*, *93*, 546–553. doi: 10.1016/j.atmosres.2008.10.005
- Brooks, H. E., Lee, J. W., & Craven, J. P. (2003). The spatial distribution of severe thunderstorm and tornado environments from global reanalysis data. *Atmospheric Research*, *67-68*, 73–94. doi: 10.1016/S0169-8095(03)00045-0
- Capotondi, A., Deser, C., Phillips, A. S., Okumura, Y., & Larson, S. M. (2020). ENSO and Pacific Decadal Variability in the Community Earth System Model Version 2. *Journal of Advances in Modeling Earth Systems*, *12*(12), e2019MS002022. doi: 10.1029/2019MS002022
- Carlson, T. N., Benjamin, S. G., Forbes, G. S., & Li, Y.-F. (1983). Elevated Mixed Layers in the Regional Severe Storm Environment: Conceptual Model and Case Studies. *Monthly Weather Review*, *111*(7), 1453–1474. doi:

- 10.1175/1520-0493(1983)111<1453:EMLITR>2.0.CO;2
- 719
720 Chen, J., Dai, A., Zhang, Y., & Rasmussen, K. L. (2020). Changes in Convective
721 Available Potential Energy and Convective Inhibition under Global Warming.
722 *Journal of Climate*, *33*(6), 2025–2050. doi: 10.1175/JCLI-D-19-0461.1
- 723 Colby, F. P. (1984). Convective Inhibition as a Predictor of Convection during AVE-
724 SESAME II. *Monthly Weather Review*, *112*(11), 2239–2252. doi: 10.1175/1520-
725 -0493(1984)112<2239:CIAAPO>2.0.CO;2
- 726 Craven, J. P., & Brooks, H. E. (2004). Baseline Climatology of Sounding Derived
727 Parameters Associated With Deep Moist Convection. *National Weather Di-
728 gest*, *28*, 13–24. [https://www.nssl.noaa.gov/users/brooks/public.html/
729 papers/cravenbrooksna.pdf](https://www.nssl.noaa.gov/users/brooks/public.html/papers/cravenbrooksna.pdf).
- 730 Craven, J. P., Jewell, R. E., & Brooks, H. E. (2002). Comparison between Ob-
731 served Convective Cloud-Base Heights and Lifting Condensation Level for
732 Two Different Lifted Parcels. *Weather and Forecasting*, *17*(4), 885–890. doi:
733 10.1175/1520-0434(2002)017<0885:CBOCCB>2.0.CO;2
- 734 Dai, A., Fung, I. Y., & Genio, A. D. D. (1997). Surface Observed Global Land Pre-
735 cipitation Variations during 1900–88. *Journal of Climate*, *10*(11), 2943–2962.
736 doi: 10.1175/1520-0442(1997)010<2943:SOGLPV>2.0.CO;2
- 737 Dai, A., & Wigley, T. M. L. (2000). Global patterns of ENSO-induced precipitation.
738 *Geophysical Research Letters*, *27*(9), 1283–1286. doi: 10.1029/1999GL011140
- 739 Danabasoglu, G., Lamarque, J.-F., Bacmeister, J., Bailey, D. A., DuVivier, A. K.,
740 Edwards, J., et al. (2020). The Community Earth System Model Ver-
741 sion 2 (CESM2). *Journal of Advances in Modeling Earth Systems*, *12*(2),
742 e2019MS001916. doi: 10.1029/2019MS001916
- 743 Deser, C. (2020). “Certain Uncertainty: The Role of Internal Climate Variability in
744 Projections of Regional Climate Change and Risk Management”. *Earth’s Fu-
745 ture*, *8*(12), e2020EF001854. doi: 10.1029/2020EF001854
- 746 Deser, C., Knutti, R., Solomon, S., & Phillips, A. S. (2012b). Communication of the
747 role of natural variability in future North American climate. *Nature Climate
748 Change*, *2*(11). doi: 10.1038/nclimate1562
- 749 Deser, C., Phillips, A., Bourdette, V., & Teng, H. (2012a). Uncertainty in climate
750 change projections: the role of internal variability. *Climate Dynamics*, *38*(3),
751 527–546. doi: 10.1007/s00382-010-0977-x
- 752 Diffenbaugh, N. S., Scherer, M., & Trapp, R. J. (2013). Robust increases in severe
753 thunderstorm environments in response to greenhouse forcing. *Proceedings of
754 the National Academy of Sciences*, *110*(41), 16361–16366. doi: 10.1073/pnas
755 .1307758110
- 756 Doswell, C. A., & Rasmussen, E. N. (1994). The Effect of Neglecting the Virtual
757 Temperature Correction on CAPE Calculations. *Weather and Forecasting*,
758 *9*(4), 625–629. doi: 10.1175/1520-0434(1994)009<0625:TEONTV>2.0.CO;2
- 759 Dougherty, E., & Rasmussen, K. L. (2021). Variations in Flash Flood-Producing
760 Storm Characteristics Associated with Changes in Vertical Velocity in a Future
761 Climate in the Mississippi River Basin. *Journal of Hydrometeorology*, *22*(3),
762 671–687. doi: 10.1175/JHM-D-20-0254.1
- 763 Eyring, V., Bony, S., Meehl, G. A., Senior, C. A., Stevens, B., Stouffer, R. J., &
764 Taylor, K. E. (2016). Overview of the Coupled Model Intercomparison Project
765 Phase 6 (CMIP6) experimental design and organization. *Geoscientific Model
766 Development*, *9*(5), 1937–1958. doi: 10.5194/gmd-9-1937-2016
- 767 Gensini, V. A., & Ashley, W. S. (2011). Climatology of Potentially Severe Convec-
768 tive Environments from the North American Regional Reanalysis. *Electronic J.
769 Severe Storms Meteor*, *6*(8), 1–40. doi: 10.55599/ejssm.v6i8.35
- 770 Gettelman, A., & Morrison, H. (2015). Advanced Two-Moment Bulk Micro-
771 physics for Global Models. Part I: Off-Line Tests and Comparison with
772 Other Schemes. *Journal of Climate*, *28*(3), 1268–1287. doi: 10.1175/
773 JCLI-D-14-00102.1

- 774 Golaz, J.-C., Larson, V. E., & Cotton, W. R. (2002). A PDF-Based Model for
775 Boundary Layer Clouds. Part I: Method and Model Description. *Journal of*
776 *the Atmospheric Sciences*, *59*(24), 3540–3551. doi: 10.1175/1520-0469(2002)
777 059(3540:APBMFB)2.0.CO;2
- 778 Hawkins, E., & Sutton, R. (2009). The Potential to Narrow Uncertainty in Regional
779 Climate Predictions. *Bulletin of the American Meteorological Society*, *90*(8),
780 1095–1108. doi: 10.1175/2009BAMS2607.1
- 781 Hersbach, H., Bell, B., Berrisford, P., Hirahara, S., Horányi, A., Muñoz-Sabater, J.,
782 ... Thépaut, J.-N. (2020). The ERA5 global reanalysis. *Quarterly Journal of*
783 *the Royal Meteorological Society*, *146*(730), 1999–2049. doi: 10.1002/qj.3803
- 784 Higgins, R. W., Yao, Y., Yarosh, E. S., Janowiak, J. E., & Mo, K. C. (1997). In-
785 fluence of the Great Plains Low-Level Jet on Summertime Precipitation and
786 Moisture Transport over the Central United States. *Journal of Climate*, *10*(3),
787 481–507. doi: 10.1175/1520-0442(1997)010(0481:IOTGPL)2.0.CO;2
- 788 Holton, J. R., & Hakim, G. J. (2013). Chapter 9 - Mesoscale Circulations. In *An In-*
789 *troduction to Dynamic Meteorology* (Fifth ed., p. 279-323). Boston: Academic
790 Press. doi: 10.1016/B978-0-12-384866-6.00009-X
- 791 Hoogewind, K. A., Baldwin, M. E., & Trapp, R. J. (2017). The Impact of Cli-
792 mate Change on Hazardous Convective Weather in the United States: Insight
793 from High-Resolution Dynamical Downscaling. *Journal of Climate*, *30*(24),
794 10081–10100. doi: 10.1175/JCLI-D-16-0885.1
- 795 Hurrell, J. W., Holland, M. M., Gent, P. R., Ghan, S., Kay, J. E., Kushner, P. J.,
796 ... Marshall, S. (2013). The Community Earth System Model: A Framework
797 for Collaborative Research. *Bulletin of the American Meteorological Society*,
798 *94*(9), 1339–1360. doi: 10.1175/BAMS-D-12-00121.1
- 799 IPCC. (2021). Summary for policymakers. In *Climate Change 2021: The Physical*
800 *Science Basis. Contribution of Working Group I to the Sixth Assessment Re-*
801 *port of the Intergovernmental Panel on Climate Change* (p. 332). Cambridge,
802 United Kingdom and New York, NY, USA: Cambridge University Press. doi:
803 10.1017/9781009157896.001
- 804 Johns, R. H., & Doswell, C. A. (1992). Severe Local Storms Forecasting. *Weather*
805 *and Forecasting*, *7*(4), 588–612. doi: 10.1175/1520-0434(1992)007(0588:SLSF)2
806 .0.CO;2
- 807 Kelly, D. L., Schaefer, J. T., & Doswell, C. A. (1985). Climatology of Nontornadic
808 Severe Thunderstorm Events in the United States. *Monthly Weather Review*,
809 *113*(11), 1997–2014. doi: 10.1175/1520-0493(1985)113(1997:CONSTE)2.0.CO;
810 2
- 811 Kirtman, B. P., Min, D., Infanti, J. M., Kinter, J. L., Paolino, D. A., Zhang, Q., ...
812 Wood, E. F. (2014). The North American Multimodel Ensemble: Phase-1
813 Seasonal-to-Interannual Prediction; Phase-2 toward Developing Intraseasonal
814 Prediction. *Bulletin of the American Meteorological Society*, *95*(4), 585–601.
815 doi: 10.1175/BAMS-D-12-00050.1
- 816 Klemp, J. B. (1987). Dynamics of Tornadic Thunderstorms. *Annual Review of Fluid*
817 *Mechanics*, *19*(1), 369–402. doi: 10.1146/annurev.fl.19.010187.002101
- 818 Lee, S.-K., Atlas, R., Enfield, D., Wang, C., & Liu, H. (2013). Is There an Optimal
819 ENSO Pattern That Enhances Large-Scale Atmospheric Processes Conducive
820 to Tornado Outbreaks in the United States? *Journal of Climate*, *26*(5), 1626–
821 1642. doi: 10.1175/JCLI-D-12-00128.1
- 822 Lepore, C., Abernathy, R., Henderson, N., Allen, J. T., & Tippet, M. K. (2021).
823 Future Global Convective Environments in CMIP6 Models. *Earth's Future*,
824 *9*(12), e2021EF002277. doi: 10.1029/2021EF002277
- 825 Li, F., Chavas, D. R., Reed, K. A., & Dawson II, D. T. (2020). Climatology of
826 Severe Local Storm Environments and Synoptic-Scale Features over North
827 America in ERA5 Reanalysis and CAM6 Simulation. *Journal of Climate*,
828 *33*(19), 8339–8365. doi: 10.1175/JCLI-D-19-0986.1

- 829 Li, W., Li, L., Fu, R., Deng, Y., & Wang, H. (2011). Changes to the North At-
830 lantic Subtropical High and Its Role in the Intensification of Summer Rainfall
831 Variability in the Southeastern United States. *Journal of Climate*, *24*(5),
832 1499–1506. doi: 10.1175/2010JCLI3829.1
- 833 Lilly, D. K. (1979). The Dynamical Structure and Evolution of Thunderstorms and
834 Squall Lines. *Annual Review of Earth and Planetary Sciences*, *7*, 117. doi: 10
835 .1146/annurev.ea.07.050179.001001
- 836 Liu, C., Ikeda, K., Rasmussen, R., Barlage, M., Newman, A. J., Prein, A. F., ...
837 Yates, D. (2017). Continental-scale convection-permitting modeling of the cur-
838 rent and future climate of North America. *Climate Dynamics*, *49*(1), 71–95.
839 doi: 10.1007/s00382-016-3327-9
- 840 Ludlam, F. H. (1963). Severe Local Storms: A Review. In *Severe Local Storms*
841 *Meteorological Monographs* (Vol. 5, pp. 1–32). American Meteorological Soci-
842 ety. doi: 10.1007/978-1-940033-56-3.1
- 843 Mankin, J. S., Lehner, F., Coats, S., & McKinnon, K. A. (2020). The Value of
844 Initial Condition Large Ensembles to Robust Adaptation Decision-Making.
845 *Earth's Future*, *8*(10). doi: 10.1029/2020EF001610
- 846 Milinski, S., Maher, N., & Olonscheck, D. (2020). How large does a large ensemble
847 need to be? *Earth System Dynamics*, *11*(4), 885–901. doi: 10.5194/esd-11-885
848 -2020
- 849 Mulholland, J. P., Nesbitt, S. W., Trapp, R. J., Rasmussen, K. L., & Salio, P. V.
850 (2018). Convective Storm Life Cycle and Environments near the Sierras de
851 Córdoba, Argentina. *Monthly Weather Review*, *146*(8), 2541–2557. doi:
852 10.1175/MWR-D-18-0081.1
- 853 NCEI. (2021). NOAA National Centers for Environmental Information (NCEI) U.S.
854 Billion-Dollar Weather and Climate Disasters.
855 doi: 10.25921/stkw-7w73
- 856 Neale, R. B., & Gettelman, A. (2012). Description of the NCAR Community Atmo-
857 sphere Model (CAM 5.0) (No. NCAR/TN-486+STR). University Corporation
858 for Atmospheric Research.
859 doi: 10.5065/wgtk-4g06
- 860 Nesbitt, S. W., Salio, P. V., Ávila, E., Bitzer, P., Carey, L., Chandrasekar, V., ...
861 Grover, M. A. (2021). A Storm Safari in Subtropical South America: Proyecto
862 RELAMPAGO. *Bulletin of the American Meteorological Society*, *102*(8),
863 E1621–E1644. doi: 10.1175/BAMS-D-20-0029.1
- 864 O'Neill, B. C., Tebaldi, C., van Vuuren, D. P., Eyring, V., Friedlingstein, P., Hurtt,
865 G., ... Sanderson, B. M. (2016). The Scenario Model Intercomparison Project
866 (ScenarioMIP) for CMIP6. *Geoscientific Model Development*, *9*(9), 3461–3482.
867 doi: 10.5194/gmd-9-3461-2016
- 868 Otto-Bliesner, B. L., Brady, E. C., Fasullo, J., Jahn, A., Landrum, L., Steven-
869 son, S., ... Strand, G. (2016). Climate Variability and Change since 850
870 CE: An Ensemble Approach with the Community Earth System Model.
871 *Bulletin of the American Meteorological Society*, *97*(5), 735–754. doi:
872 10.1175/BAMS-D-14-00233.1
- 873 Pitchford, K. L., & London, J. (1962). The Low-Level Jet as Related to Nocturnal
874 Thunderstorms over Midwest United States. *Journal of Applied Meteorol-
875 ogy and Climatology*, *1*(1), 43–47. doi: 10.1175/1520-0450(1962)001<0043:
876 TLLJAR>2.0.CO;2
- 877 Rasmussen, E. N., & Blanchard, D. O. (1998). A Baseline Climatology of Sounding-
878 Derived Supercell and Tornado Forecast Parameters. *Weather and Forecasting*,
879 *13*(4), 1148–1164. doi: 10.1175/1520-0434(1998)013<1148:ABCOSD>2.0.CO;2
- 880 Rasmussen, K. L., & Houze, R. A. (2011). Orographic Convection in Subtropical
881 South America as Seen by the TRMM Satellite. *Monthly Weather Review*,
882 *139*(8), 2399–2420. doi: 10.1175/MWR-D-10-05006.1

- 883 Rasmussen, K. L., & Houze, R. A. (2016). Convective Initiation near the Andes in
 884 Subtropical South America. *Monthly Weather Review*, *144*(6), 2351–2374. doi:
 885 10.1175/MWR-D-15-0058.1
- 886 Rasmussen, K. L., Prein, A. F., Rasmussen, R. M., Ikeda, K., & Liu, C. (2017).
 887 Changes in the convective population and thermodynamic environments in
 888 convection-permitting regional climate simulations over the United States.
 889 *Climate Dynamics*, *55*(1), 383–408. doi: 10.1007/s00382-017-4000-7
- 890 Rasmussen, K. L., Zuluaga, M. D., & Houze Jr., R. A. (2014). Severe convection and
 891 lightning in subtropical south america. *Geophysical Research Letters*, *41*(20),
 892 7359–7366. doi: 10.1002/2014GL061767
- 893 Riemann-Campe, K., Fraedrich, K., & Lunkeit, F. (2009). Global climatology of
 894 Convective Available Potential Energy (CAPE) and Convective Inhibition
 895 (CIN) in ERA-40 reanalysis. *Atmospheric Research*, *93*(1), 534–545. doi:
 896 10.1016/j.atmosres.2008.09.037
- 897 Rochette, S. M., Moore, J. T., & Market, P. S. (1999). The importance of parcel
 898 choice in elevated CAPE computations. *Natl. Wea. Dig*, *23*(4), 20–32.
- 899 Rodgers, K. B., Lee, S.-S., Rosenbloom, N., Timmermann, A., Danabasoglu,
 900 G., Deser, C., et al. (2021). Ubiquity of human-induced changes in
 901 climate variability. *Earth System Dynamics*, *12*(4), 1393–1411. doi:
 902 10.5194/esd-12-1393-2021
- 903 Ropelewski, C. F., & Halpert, M. S. (1986). North American Precipitation
 904 and Temperature Patterns Associated with the El Niño/Southern Oscil-
 905 lation (ENSO). *Monthly Weather Review*, *114*(12), 2352–2362. doi:
 906 10.1175/1520-0493(1986)114<2352:NAPATP>2.0.CO;2
- 907 Rotunno, R. (1981). On the Evolution of Thunderstorm Rotation. *Monthly Weather*
 908 *Review*, *109*(3), 577–586. doi: 10.1175/1520-0493(1981)109<0577:OTEOTR>2.0
 909 .CO;2
- 910 Rotunno, R., Klemp, J. B., & Weisman, M. L. (1988). A Theory for Strong, Long-
 911 Lived Squall Lines. *Journal of the Atmospheric Sciences*, *45*(3), 463–485. doi:
 912 10.1175/1520-0469(1988)045<0463:ATFSL>2.0.CO;2
- 913 Seeley, J. T., & Romps, D. M. (2015). The Effect of Global Warming on Severe
 914 Thunderstorms in the United States. *Journal of Climate*, *28*(6), 2443–2458.
 915 doi: 10.1175/JCLI-D-14-00382.1
- 916 Skamarock, W. C., Klemp, J. B., Dudhia, J., Gill, D. O., Barker, D. M., Duda,
 917 M. G., ... Powers, J. G. (2008). A Description of the Advanced Research
 918 WRF Version 3 (No. NCAR/TN-475+STR). University Corporation for Atmo-
 919 spheric Research.
 920 doi: 10.5065/D68S4MVH
- 921 Taszarek, M., Allen, J. T., Marchio, M., & Brooks, H. E. (2021). Global climatology
 922 and trends in convective environments from ERA5 and rawinsonde data. *npj*
 923 *Climate and Atmospheric Science*, *4*(1), 1–11. doi: 10.1038/s41612-021-00190
 924 -x
- 925 Taylor, K. E., Stouffer, R. J., & Meehl, G. A. (2012). An Overview of CMIP5
 926 and the Experiment Design. *Bulletin of the American Meteorological Society*,
 927 *93*(4), 485–498. doi: 10.1175/BAMS-D-11-00094.1
- 928 Thompson, D. B., & Roundy, P. E. (2013). The Relationship between the
 929 Madden–Julian Oscillation and U.S. Violent Tornado Outbreaks in the
 930 Spring. *Monthly Weather Review*, *141*(6), 2087–2095. doi: 10.1175/
 931 MWR-D-12-00173.1
- 932 Ting, M., Kossin, J. P., Camargo, S. J., & Li, C. (2019). Past and Future Hurricane
 933 Intensity Change along the U.S. East Coast. *Scientific Reports*, *9*(1), 7795.
 934 doi: 10.1038/s41598-019-44252-w
- 935 Trapp, R. J., Diffenbaugh, N. S., Brooks, H. E., Baldwin, M. E., Robinson, E. D.,
 936 & Pal, J. S. (2007). Changes in severe thunderstorm environment frequency
 937 during the 21st century caused by anthropogenically enhanced global radiative

- 938 forcing. *Proceedings of the National Academy of Sciences*, 104(50), 19719–
 939 19723. doi: 10.1073/pnas.0705494104
- 940 Trapp, R. J., Dittenbaugh, N. S., & Gluhovsky, A. (2009). Transient response of se-
 941 vere thunderstorm forcing to elevated greenhouse gas concentrations. *Geophys-*
 942 *ical Research Letters*, 36(1). doi: 10.1029/2008GL036203
- 943 Weisman, M. L., & Rotunno, R. (2000). The Use of Vertical Wind Shear versus He-
 944 licity in Interpreting Supercell Dynamics. *Journal of the Atmospheric Sciences*,
 945 57(9), 1452–1472. doi: 10.1175/1520-0469(2000)057<1452:TUOVWS>2.0.CO;2
- 946 Zhang, G., & McFarlane, N. A. (1995). Sensitivity of climate simulations to
 947 the parameterization of cumulus convection in the Canadian climate cen-
 948 tre general circulation model. *Atmosphere-Ocean*, 33(3), 407–446. doi:
 949 10.1080/07055900.1995.9649539
- 950 Zipser, E. J., Cecil, D. J., Liu, C., Nesbitt, S. W., & Yorty, D. P. (2006). WHERE
 951 ARE THE MOST INTENSE THUNDERSTORMS ON EARTH? *Bulletin of*
 952 *the American Meteorological Society*, 87(8), 1057–1072. doi: 10.1175/BAMS-87
 953 -8-1057

Abstract

Hazards from convective weather pose a serious threat to the continental United States (CONUS) every year. Previous studies have examined how future projected changes in climate might impact the frequency and intensity of severe weather using simulations with both convection-permitting regional models and coarser climate and Earth system models. However, many of these studies have been limited to single representations of the future climate state with little insight into the uncertainty of how the population of convective storms may evolve. To thoroughly explore this aspect, a large ensemble of Earth system model simulations was implemented to investigate how forced responses in large-scale convective environments might be modulated by internal climate variability. Daily data from an ensemble of 50 simulations with the most recent version of the Community Earth System Model was used to examine changes in the severe weather environment over the eastern CONUS during boreal spring from 1870-2100. Results indicate that forced changes in convective environments were small between 1870 and 1990, but throughout the 21st century, convective available potential energy and atmospheric stability (convective inhibition) is projected to increase while 0-6 km vertical wind shear decreases. Internal climate variability can either significantly enhance or suppress these forced changes. The time evolution of bivariate distributions of convective indices illustrates that future springtime convective environments over the eastern CONUS will be characterized by relatively less frequent, less organized, but deeper, more intense convection. Future convective environments will also be less supportive of the most severe convective modes and associated hazards.

Plain Language Summary

Understanding to what extent climate change will alter severe weather is critical for planning and resilience. Moreover, natural variations in climate could either enhance or suppress climate change signals, so documenting the range of equally plausible future outcomes is important. Utilizing a large number of simulations from a climate model, we document projected changes in large-scale atmospheric conditions critical to severe weather from both climate change and natural variability. The impact of climate change on these environments became apparent late in the 20th century and will likely strengthen over the coming decades. Convective environments over the eastern U.S. will increasingly be supportive of less frequent, less organized, but more explosive storms due to increases in mid-level stability and positively buoyant energy, but slight decreases in vertical wind shear. However, such changes may be significantly modified by natural climate variability, resulting in a wide range of possible outcomes.

1 Introduction and Motivation

Few places around the globe experience extreme severe weather like the United States (U.S.). Particularly over the central and eastern U.S., the peak in severe weather is largely due to synoptic-scale interactions with the Rocky Mountains. During the boreal spring season, the Bermuda High, as well as the nocturnal Great Plains Low-Level Jet (GPLLJ), enhances a southerly flow of warm, moist air from the Gulf of Mexico into the Great Plains (Pitchford & London, 1962; Higgins et al., 1997; W. Li et al., 2011). This moist air, trapped by the mountains to the west, creates a strong gradient between the dry, western desert air and provides the necessary ingredients for high convective energy downstream. In addition, the terrain of the Rockies helps to produce a mid-level capping inversion as the hot, dry, mixed-layer air is advected off the elevated plateaus, which can then be further enhanced as the climatological westerly flow aloft descends the lee-side of the mountains (Carlson et al., 1983). This inversion suppresses convective activity and further facilitates the daily accumulation of convective energy increasing to very high levels. If the inversion is then broken, enhanced lifting and deep convection can occur.

63 In the year 2021 alone, 20 destructive meteorological events occurred in the U.S.
64 each resulting in \$1 billion or more of damages. Eleven of these events were due to se-
65 vere weather and included hazards such as tornadoes, large hail, and strong winds (NCEI,
66 2021). Records from the National Climatic Data Center indicate that, over the last decade,
67 the occurrence of billion-dollar severe weather events has more than doubled. Addition-
68 ally, the Intergovernmental Panel on Climate Change (IPCC) has noted with high confi-
69 dence that models consistently project changes in climate that support an increase in
70 the frequency and intensity of severe weather (IPCC, 2021). As temperatures increase
71 due to enhanced greenhouse gas concentrations, the air-column moisture content also in-
72 creases, thus leading to an increase in convective available potential energy - a key in-
73 gredient for the development of severe weather. In the current climate, hazards associ-
74 ated with severe storms already threaten lives, infrastructure, and food and water sup-
75 plies within the U.S. and elsewhere. With this in mind, an improved understanding of
76 the causes of both near-term and longer-timescale variability in severe weather could aid
77 in improving the accuracy of future predictions, as well as enhance resilience to severe
78 weather outbreaks.

79 Due to their relatively small scale and intermittent occurrence, observing and col-
80 lecting homogeneous records of severe weather events is difficult, especially when these
81 events occur in relatively unpopulated or rural areas (Johns & Doswell, 1992; Brooks et
82 al., 2003). To partially offset the lack of direct, long-term, and reliable observations of
83 severe storm events, the severe weather research community has developed convective
84 indices and covariate proxies that represent the thermodynamic and kinematic compo-
85 nents of the local storm environment and are indicative of conditions favorable for se-
86 vere weather events (Ludlam, 1963; E. N. Rasmussen & Blanchard, 1998; Craven & Brooks,
87 2004). Consideration of these diagnostic variables can aid in determining the historical
88 occurrence and future probability of severe weather, including the frequency, intensity,
89 and type, or mode, of convection.

90 Convective Available Potential Energy (CAPE) is a measure of the potential en-
91 ergy available for upward vertical motion in a storm environment, while Convective In-
92 hibition (CIN) is indicative of the boundary layer stability, which inhibits upward ver-
93 tical motion. Considerable prior research has investigated both the recent historical cli-
94 matology as well as projections of the future evolution of these parameters. In general,
95 these studies have shown that boreal spring CAPE is expected to increase substantially
96 over the eastern continental U.S. (CONUS) by the end of the 21st century, largely as a
97 result of an increase in specific humidity and warmer temperatures (e.g., Trapp et al.,
98 2007, 2009; Diffenbaugh et al., 2013; Seeley & Romps, 2015; Hoogewind et al., 2017; K. L. Ras-
99 mussen et al., 2017; Chen et al., 2020; Lepore et al., 2021). Although less explored, the
100 spatiotemporal evolution of boreal spring CIN is also consistent among previous stud-
101 ies, with increasing boundary layer stability (increasing CIN magnitudes) by 2100, par-
102 ticularly over the central CONUS (e.g., Hoogewind et al., 2017; K. L. Rasmussen et al.,
103 2017; Chen et al., 2020; Lepore et al., 2021). While many of these studies have utilized
104 large-scale climate models to explore future changes in these convective indices, others
105 have taken a different approach by applying dynamical downscaling or the pseudo-global
106 warming approach (Hoogewind et al., 2017; Chen et al., 2020). For example, K. L. Ras-
107 mussen et al. (2017) analyzed high-resolution convection-permitting simulations (Liu et
108 al., 2017) using the regional Weather Research and Forecasting model (WRF; Skamarock
109 et al., 2008) at 4 km resolution forced with ERA-Interim Reanalysis plus a climate change
110 perturbation from climate model simulations to investigate how CAPE, CIN, and their
111 subsequent convective populations may change in the future. In particular, they calcu-
112 lated end-of-century monthly anomalies of CAPE and CIN relative to the historical cli-
113 matology (1976-2005) using a 19-model ensemble-mean from phase 5 of the Coupled Model
114 Intercomparison Project (CMIP5; Taylor et al., 2012) under a strong, future emissions
115 scenario. Their results are broadly consistent with the aforementioned studies, with in-
116 creases projected in spring and summer CAPE and increasing magnitudes of CIN (in-

117 creased stability) over the eastern CONUS. Such findings suggest that in the future, weak
118 to moderate storms will be less frequent because of increased stability, but the most in-
119 tense storms will become more numerous (K. L. Rasmussen et al., 2017).

120 In contrast, there is less agreement on projected end-of-century changes in tropo-
121 spheric wind shear, which is a key factor for storm organization, longevity, and severe
122 weather development. For instance, Trapp et al. (2007), Diffenbaugh et al. (2013), and
123 Ting et al. (2019) used a variety of Earth system models with RCP8.5 forcing and found
124 a robust swath of decreasing wind shear over most of the CONUS during the boreal spring
125 season, while Hoogewind et al. (2017) and Lepore et al. (2021) both found increasing wind
126 shear over the western and central U.S. with decreasing shear over the eastern U.S. by
127 2100 also using Earth system models.

128 While changes in individual convective indices are useful for analyzing specific char-
129 acteristics of severe storms, integrated measures of changes in storm environments, such
130 as the product of CAPE and the wind shear between the surface and 6-km (S06), can
131 provide a more complete spatiotemporal description of the convective environment. By
132 definition, CAPES06 considers both the thermodynamic energy and the kinematic mo-
133 tion in a storm environment. As a result, increases in this variable could signify an in-
134 crease in the frequency of significant severe storms relative to non-severe storms (E. N. Ras-
135 mussen & Blanchard, 1998; Brooks et al., 2003; Brooks, 2009). The historical climatol-
136 ogy of warm-season CAPES06 produces a large-scale, spatially coherent pattern over the
137 eastern CONUS, reflecting the climatology of the CAPE index (Brooks et al., 2003; F. Li
138 et al., 2020). Simulations of future projections suggest that CAPES06 will mirror changes
139 in CAPE. For instance, Seeley and Romps (2015) used a subset of climate models from
140 the CMIP5, chosen based on their ability to reproduce a radiosonde climatology of se-
141 vere storm environments, to compare 21st century changes in the frequency of environ-
142 ments favorable for severe weather using a CAPES06 threshold. In general, all four mod-
143 els produced changes for end-of-century CAPES06 that showed consistent spatial pat-
144 terns with increases over the southern and central U.S. ranging from 50 to 180% of the
145 historical climatology (Seeley & Romps, 2015).

146 Another approach has been to consider combinations of convective indices to de-
147 termine the Number of Days with SEVere weather environments (NDSEV; Brooks et al.,
148 2003). Previous studies agree that NDSEV will increase over much of the U.S. during
149 the boreal spring season, but differences exist in the projected magnitudes of the increases.
150 For instance, Trapp et al. (2007, 2009) and Diffenbaugh et al. (2013) find an increase of
151 ~ 3 days per season over the central and eastern CONUS by 2100 utilizing an Earth sys-
152 tem model, whereas Hoogewind et al. (2017) found an increase of ~ 10 days per season
153 using a dynamical downscaling approach. Such discrepancies are likely a consequence
154 of varying definitions used for the NDSEV parameter, contrasting time periods between
155 the studies, as well as model grid-spacing and emission scenario differences.

156 The aforementioned studies have provided valuable insights and have set the founda-
157 tion for the types of changes that are likely to be experienced in future convective en-
158 vironments during the boreal spring over the U.S. However, they primarily use either a
159 small number of simulations from a single model, short integration periods (~ 30 years),
160 or multi-model ensemble means with different emission scenarios and other model vari-
161 ations to compare changes in convective environments due to anthropogenic forcing. An
162 additional and important perspective can be gained by utilizing a large ensemble approach
163 from a single model, whereby many simulations of the future are run under the same ra-
164 diative forcing scenario but are started from slightly different initial conditions. The sig-
165 nificance of this approach arises from the presence of unpredictable, internal (or natu-
166 ral) climate variability, which results in a range of possible future outcomes, all of which
167 can be considered a possible reality (e.g., Deser et al., 2012a). Internal variability is one
168 of the largest factors of unavoidable uncertainty in regional climate projections and can
169 either enhance or suppress a forced signal (Deser, 2020). It is important to note that each

170 simulation in a large ensemble contains a common response to the radiative forcing su-
171 perimposed upon a different sequence of internal variability. In general, internal climate
172 variability is larger in the extra-tropics than in the tropics and is relatively stronger com-
173 pared to forced variability when examining climate change several decades into the fu-
174 ture (Hawkins & Sutton, 2009; Deser et al., 2012a; Milinski et al., 2020), as has been done
175 here.

176 Sub-seasonal to decadal variability is often associated with leading modes of cli-
177 mate variability. A handful of studies have examined the relationship between severe weather
178 and modes of climate variability such as the El Niño Southern Oscillation (ENSO; Lee
179 et al., 2013; Allen et al., 2015) and the Madden Julian Oscillation (MJO; Thompson &
180 Roundy, 2013). Allen et al. (2015) found that fewer tornado and hail events occur over
181 the central U.S. during El Niño events than during La Niña events. Thompson and Roundy
182 (2013) showed that violent tornado outbreaks in the months March-May are more than
183 two times more frequent during the second phase of the Real-time Multivariate MJO (RMM)
184 index than during any other phases or during MJO inactivity. These results are criti-
185 cal in helping to both better understand the patterns of severe weather outbreaks as well
186 as improve the skill for long-range seasonal predictions of severe weather events (Allen
187 et al., 2015). However, how low-frequency, unforced climate variability modulates the
188 convective mode (i.e. frequency and storm type), as well as the thermodynamic and kine-
189 matic environment critical for severe weather, has not been examined extensively to date,
190 even though it is likely an important influence regionally.

191 As such, this study builds on the previous literature, specifically by taking advan-
192 tage of a recently released large ensemble of simulations from the Community Earth Sys-
193 tem Model version 2.0 (CESM2; Danabasoglu et al., 2020), hereafter referred to as the
194 CESM2-LE (Rodgers et al., 2021). Leveraging the CESM2-LE, which extends from 1870-
195 2100, allows us to evaluate the temporal evolution of convective environments over a much
196 longer, continuous-time record than has been examined before. Further, it allows us to
197 robustly examine both the forced variability due to anthropogenic climate change, as well
198 as the possible role of internal variability in modulating the forced signal over the com-
199 ing decades. To our knowledge, these aspects related to severe weather environments over
200 the U.S. have yet to be rigorously examined, and thus represent a novel aspect of the
201 current study. An increased understanding of the possible combined effects of forced and
202 internal variability on convective environments is important for ensuring that climate
203 adaptation policies are based on the most complete, scientific information available (Deser,
204 2020; Mankin et al., 2020).

205 **2 Methodology**

206 We utilize simulation data from the CESM (Hurrell et al., 2013; Danabasoglu et
207 al., 2020). The open-source CESM is unique in that it is both developed and applied to
208 scientific problems by a large community of researchers. It is a critical infrastructure for
209 the U.S. climate research community and is principally funded by the National Science
210 Foundation (NSF) and managed by the U.S. National Center for Atmospheric Research
211 (NCAR). Simulations performed with the CESM have made many significant contribu-
212 tions to climate research, ranging from paleoclimate applications (e.g., Otto-Bliesner et
213 al., 2016) to contributions to the North American Multi-Model Ensemble (NMME; Kirt-
214 man et al., 2014) seasonal forecasting effort led by the National Oceanic and Atmospheric
215 Administration (NOAA). Simulations with CESM have also been used extensively in both
216 national and international assessments of climate science, including substantial contri-
217 butions to version 6 of the CMIP (CMIP6; Eyring et al., 2016). The salient point is that
218 CESM provides the broader academic community with a core modeling system to inves-
219 tigate a diverse set of earth system interactions across multiple time and space scales.

220

2.1 Model Information and Data

221

222

223

224

225

226

227

228

229

230

231

232

233

234

235

236

237

238

Daily data for specific humidity, column air temperature, near-surface (10-meter) wind speed, zonal and meridional winds, and geopotential heights were obtained from a large ensemble (LE) produced with the coupled CESM2 (Danabasoglu et al., 2020). The CESM2-LE uses the Community Atmosphere Model version 6 (CAM6), which is a ‘low-top’ model consisting of 32 vertical levels (a relatively coarse stratospheric representation) and a nominal 1° (1.25° in longitude and 0.9° in latitude) spatial resolution. To study the temporal evolution of the severe weather environment over the CONUS during boreal spring, 50 ensemble members were analyzed spanning 1870-2100. Each ensemble member used CMIP6 forcings over the historical record and a future (2015-2100) forcing of SSP3-7.0 (Rodgers et al., 2021), a medium-high emissions scenario resulting in approximately 7.0 Wm^{-2} in radiative forcing by the end of the 21st century (O’Neill et al., 2016; IPCC, 2021). This level of forcing is currently a policy-relevant target, and it is a more moderate forcing scenario than those analyzed in most of the aforementioned studies that have examined future changes in convective indices. An ensemble of this size and duration with a CMIP6 generation Earth system model provides an unprecedented opportunity to investigate the long-term evolution of large-scale convective environments, how it is impacted by forced variability, and to what extent the latter is influenced by internal climate variability.

239

2.2 Convective Parameters

240

241

242

243

244

245

246

247

248

249

The CESM2-LE simulations were used to compute several parameters to quantify the thermodynamic and kinetic characteristics of the large-scale storm environment across the U.S. Closely associated with the potential occurrence of deep convection is CAPE (Jkg^{-1}) (Doswell & Rasmussen, 1994; Riemann-Campe et al., 2009). This thermodynamic parameter is formally defined as the vertical integral of buoyancy from the level of free convection (LFC) to the equilibrium level, making it suitable to diagnose conditional instability and potential updraft strength (Holton & Hakim, 2013). We have chosen to use the most-unstable CAPE in the lowest 3000 meters to ensure that our analysis captures potentially elevated convection, as well as the maximum instability (Rochette et al., 1999).

250

251

252

253

254

255

256

257

The CIN (Jkg^{-1}) is equal to the negative buoyancy, or the negative work done by the atmospheric boundary layer as a parcel ascends from the surface, through the stable layer, and to the LFC (Colby, 1984; E. N. Rasmussen & Blanchard, 1998; Riemann-Campe et al., 2009). It is routinely analyzed to evaluate the stability of the local atmosphere and the potential suppression of convective motions. As CIN is the amount of energy an air parcel needs to overcome in order to reach the LFC, it is commonly referred to as a negative value (i.e., more negative values mean more convective inhibition or more stability), but will be discussed here as changes in magnitude.

258

259

260

261

262

263

264

265

266

267

268

269

270

To explore the kinematic components of the convective environment, we used the difference in the bulk vertical wind shear from 10 meters above ground level to 6-km (~ 525 hPa) altitude, known as S06 (ms^{-1}). Past work suggests that while lower-level wind shear is important for tornadic environments, S06 is one of the best indices for determining storm type and organization (E. N. Rasmussen & Blanchard, 1998; Weisman & Rotunno, 2000; Brooks et al., 2003). Large values of S06 are indicative of stronger mid-level rotation such as single-celled thunderstorms. In addition, higher S06 allows for increased organization for storm dynamics such as a tilted updraft, which is necessary to displace the area of upward vertical motion from the downward vertical motion. This increases the potential for the storm to form a mesocyclone and develop into a supercell, which is typically accompanied by severe weather hazards. Sufficient S06 is also essential for multi-cell organized systems, such as squall lines, as it helps to counteract the low-level circulation induced by the cold pool (Rotunno et al., 1988). As a cold pool is produced

271 by evaporative cooling near the surface, new cells are triggered along the gust front. The
 272 triggering and subsequent growth of these new cells are highly dependent on the amount
 273 of low-level wind shear, making it crucial to the longevity of a multi-cellular organized
 274 system.

275 A covariate convective index used here is the product of CAPE and S06, or CAPES06
 276 (m^3s^{-3}). Previous research has demonstrated the effectiveness of CAPES06 to help dis-
 277 criminate between significant severe storms and less severe storms (E. N. Rasmussen &
 278 Blanchard, 1998; Craven et al., 2002; Brooks et al., 2003; Brooks, 2009; Seeley & Romps,
 279 2015). As CAPES06 takes into account two of the most necessary components for con-
 280 vection, the thermodynamic energy and the vertical kinematic structure, high values of
 281 this parameter are indicative of increased storm organization and higher updraft veloci-
 282 ties. Historically, soundings from days with the most severe storms exhibited high val-
 283 ues in this index (e.g., E. N. Rasmussen & Blanchard, 1998; Brooks et al., 2003; Brooks,
 284 2009).

285 Finally, to convey the integrated effects of the convective indices, changes in ND-
 286 SEV are also examined. Following the definitions used in past studies (Brooks et al., 2003;
 287 Trapp et al., 2007; Gensini & Ashley, 2011; Hoogewind et al., 2017), a day is counted
 288 as a severe weather day when $\text{CAPE} \geq 100 \text{ Jkg}^{-1}$, $\text{CIN} \geq -100 \text{ Jkg}^{-1}$, $\text{S06} \geq 5 \text{ ms}^{-1}$,
 289 and $\text{CAPES06} \geq 10,000 \text{ m}^3\text{s}^{-3}$. Then, the sum of the number of days throughout the
 290 boreal spring season that meet the criteria are obtained to provide an estimate of the
 291 potential number of severe weather days per season.

292 This study will focus primarily on the eastern CONUS region outlined in Fig. 1,
 293 which is a highly active region for intense convection. Note, however, that the ocean re-
 294 gions are masked from the analysis so that the focus is on convective indices over land
 295 only. We define the spring season as March through June (MAMJ), as this period cap-
 296 tures the months when storms are most frequent and violent over the eastern CONUS
 297 (Kelly et al., 1985; Brooks et al., 2003; Gensini & Ashley, 2011; F. Li et al., 2020). Later
 298 into the summer season, the temperature and moisture gradients in this region are weaker,
 299 and the jet-stream begins to shift north, resulting in an overall northward shift in con-
 300 vective activity.

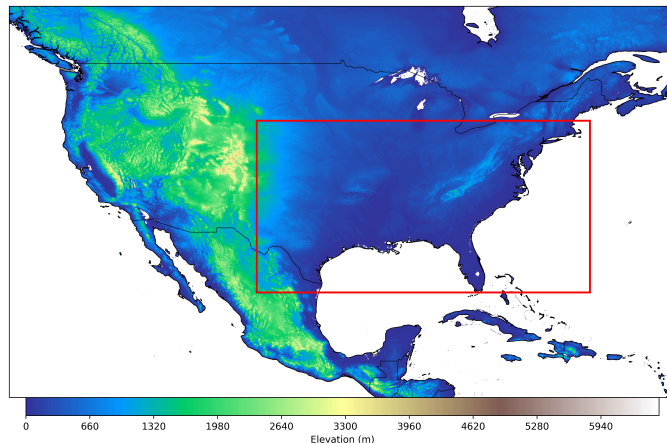


Figure 1. Red box highlights the eastern CONUS domain used for this study. Latitude bounds are between (25°N and 43°N) and longitude bounds are between (-104°W , -69°W).

301

2.3 Verification

302

303

304

305

306

307

308

309

310

311

312

313

314

315

316

317

318

319

320

321

322

323

324

325

To verify that the CESM2-LE is a viable tool for the analysis of large-scale convective environments, the fifth-generation global climate reanalysis (ERA5; Hersbach et al., 2020) from the European Centre for Medium-Range Forecast (ECMWF) was used for model validation. Previous studies have found ERA5 to be reliable in capturing the spatiotemporal climatology of convective environments (Taszarek et al., 2021). In particular, F. Li et al. (2020) conducted a climatological analysis of severe local storm environments over North America using ERA5 compared to CAM6 simulations of the historical period. They confirmed the validity of ERA5 against 69 radiosonde observations over the CONUS region with twice daily raw soundings and further confirmed the fidelity of CAM6 against ERA5. This is important because, relative to its predecessor CAM5 (Neale & Gettelman, 2012), CAM6 underwent significant modifications to the physical parameterization suite. Updates to the Zhang and McFarlane (1995) deep convection and orographic drag parameterizations were implemented into CAM6, along with the two-moment prognostic cloud microphysics from Gettelman and Morrison (2015). Additionally, the Cloud Layers Unified by Binormals (CLUBB; Golaz et al., 2002) replaced schemes for cloud macrophysics, boundary layer turbulence, and shallow convection previously used in CAM5, all of which are key parameterizations for modeling convection.

The MAMJ CAPES06 climatology from ERA5 (left) and the ensemble-mean climatology from CESM2-LE (right) is shown in Fig. 2 over the CONUS region. There is strong agreement between the CESM2-LE and ERA5 during 1980-2019, indicating that the model successfully captures the mean spatial characteristics of CAPES06 over the past 40 years. Although not shown, similarly strong agreement is found between ERA5 and CESM2-LE for the climatologies of the other convective indices (CAPE, CIN, and S06).

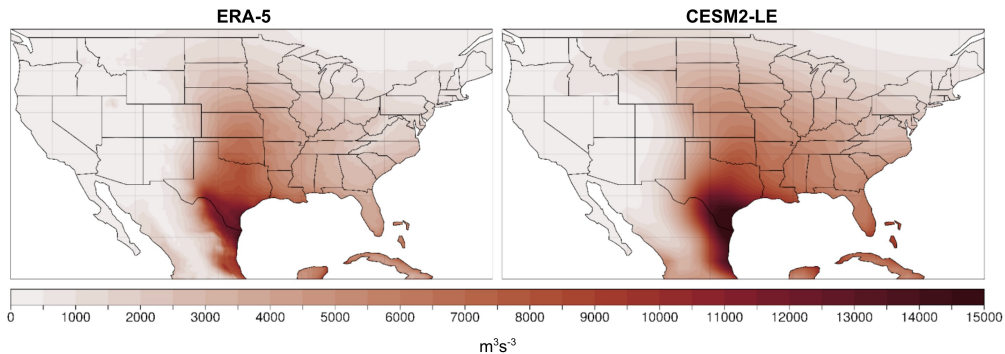


Figure 2. MAMJ CAPES06 (m^3s^{-3}) climatology for ERA5 reanalysis (left) and the CESM2-LE ensemble-mean (right) for the 1980-2019 period.

326

327

328

329

330

331

332

333

334

335

To further examine the fidelity of the CESM2-LE, we investigated the relationship between CAPES06 and ENSO, the largest driver of interannual changes in weather and climate over much of the globe (Ropelewski & Halpert, 1986; Dai et al., 1997; Allen et al., 2015; Dai & Wigley, 2000). The regression of boreal spring CAPES06 from ERA5 onto the observed Niño3.4 index over 1980-2019 is shown in Fig. 3 on the left, compared to the same quantity from the CESM2-LE over 1870-2019 on the right. Notably, CESM2-LE captures the main changes in CAPES06 associated with ENSO, including large-scale decreases in CAPES06 over the eastern CONUS during El Niño, with increases over the western CONUS. Since this study utilizes a large ensemble, many more El Niño events are sampled from the CESM2-LE data than from ERA5, resulting in more coherent spa-

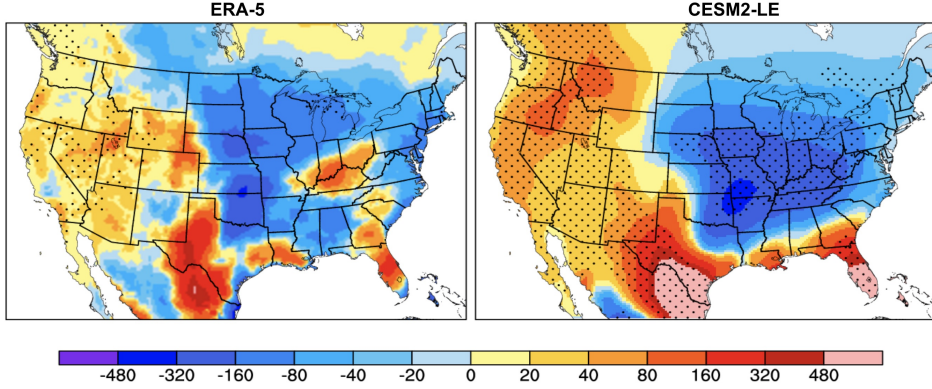


Figure 3. Regression of CAPES06 onto the ENSO index for one standard deviation over the MAMJ season from ERA5 reanalysis (1980-2019; left) and the CESM2-LE (1870-2019; right). Stippling on ERA5 shows the 95% statistical significance based on the Students T-test. Stippling on CESM2-LE indicates where 45 of the 50 members have the same sign.

336 tial patterns. This relationship is consistent with other studies that have investigated
 337 the role of ENSO on severe weather outbreaks over the U.S. during the March-May season
 338 (e.g., Lee et al., 2013; Allen et al., 2015). The results in this section, combined with
 339 the findings of earlier studies (e.g., F. Li et al., 2020), give us confidence in using the CESM2-
 340 LE to examine past and future changes in convective environments over the CONUS,
 341 as well as the variations driven by internal modes of climate variability (e.g., Capotondi
 342 et al., 2020; Rodgers et al., 2021).

343 3 Results

344 3.1 Ensemble Mean (Forced Changes)

345 The historical and future time evolution of the selected convective indices from 1870-
 346 2100 for the boreal spring season averaged over the eastern CONUS (Fig. 1) are shown
 347 in Fig. 4. The time series are expressed as seasonal anomalies relative to the 30-year base
 348 period 1971-2000. The forced component of climate change is given by the ensemble-mean
 349 of the CESM2-LE, represented by the solid black line, and the time evolution of indi-
 350 vidual ensemble members are depicted by the light gray lines. While considerable run-
 351 to-run, interannual and decadal variability is evident in individual ensemble members,
 352 the forced response in convective indices show minimal change from 1870 until about 1990,
 353 deviating little from the 30-year baseline climatologies. However, right around the year
 354 2000, forced changes in convective environments become apparent and exhibit clear de-
 355 partures from the historical climatological values throughout the current century. For
 356 instance, ensemble-mean values of CAPE steadily increase throughout the 21st century,
 357 exceeding the historical climatological values by nearly 400 Jkg^{-1} by 2100 (Fig. 4a), while
 358 the forced change in S06 becomes more negative. Specifically, anomalies in S06 reach ap-
 359 proximately -2 ms^{-1} by 2075, then remain near that level through the remainder of the
 360 century (Fig. 4b).

361 The time evolution of CAPES06 (Fig. 4c) exhibits behavior similar to that of CAPE,
 362 with an almost linear increase from 2000 of $\sim 3500 \text{ m}^3\text{s}^{-3}$ above the historical climatol-
 363 ogy by 2100. The time history of CIN also shows little deviation until this century, when
 364 it exhibits a steady decrease in magnitude to approximately -18 Jkg^{-1} by 2100 (Fig. 4d).
 365 These results show that changes in convective environments due to anthropogenic forc-
 366 ing through the end of this century are prominent and robust in CESM2-LE, as they are

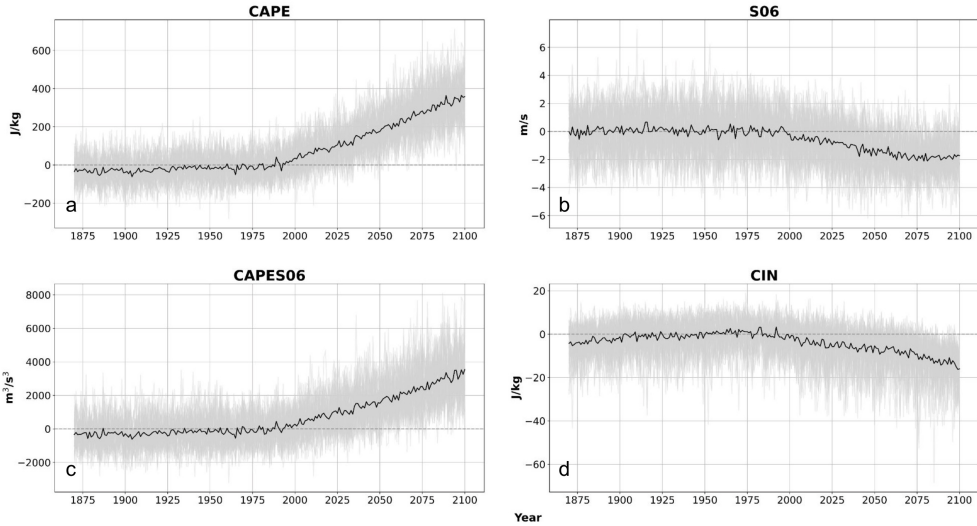


Figure 4. Time series of convective indices from 1870-2100 for (a.) CAPE (Jkg^{-1}), (b.) S06 (ms^{-1}), (c.) CAPES06 (m^3s^{-3}), and (d.) CIN (Jkg^{-1}) over the eastern CONUS region. The 50-member ensemble-mean (black) is superimposed on individual members (light grey).

367 reflected in nearly all of the 50 members of the ensemble (light grey lines in Fig. 4). Few
 368 previous studies have been able to estimate the continuous-time evolution of changes in
 369 these convective indices. One example is Diffenbaugh et al. (2013), who leveraged the
 370 CMIP5 to take regional averages over eastern CONUS for CAPE, S06, and NDSEV from
 371 1960-2100 using RCP8.5. Furthermore, Trapp et al. (2009) used a five-member ensemble
 372 from the Community Climate System Model version 3 (CCSM3) to take various re-
 373 gional averages in areas over the CONUS that frequently encounter severe weather, in-
 374 cluding the southeast, Midwest, and the southern and northern Great Plains. This was
 375 done for the same indices as Diffenbaugh et al. (2013) but from 1950-2100. In general,
 376 the trends and magnitudes of the changes in these indices are in agreement with the changes
 377 expressed in Fig. 4, especially over the southern Plains and southeast CONUS, as seen
 378 in Trapp et al. (2009). The principal point is that convective environments over the east-
 379 ern CONUS during the boreal spring are likely to undergo substantial departures from
 380 the historical record over this century (Fig. 4), moving toward higher convective energy,
 381 more stability, and less kinematic support for the production of hazards associated with
 382 severe weather.

383 To evaluate the spatial character of these changes over the CONUS, epoch differ-
 384 ences for future 30-year periods relative to the 1971-2000 baseline climatology are shown
 385 in Fig. 5. By 2100, the CESM2-LE projects spatially coherent forced changes in convec-
 386 tive environments relevant to the frequency and intensity of severe weather. Over the
 387 next few decades (2021-2050), increases in CAPE are largest near the Gulf coast and are
 388 positive across the entire CONUS (Fig. 5a). These changes in CAPE are projected to
 389 strengthen throughout the rest of this century, primarily over the eastern CONUS and
 390 southern Plains (Trapp et al., 2007; Diffenbaugh et al., 2013; Seeley & Romps, 2015; Hoogewind
 391 et al., 2017; K. L. Rasmussen et al., 2017; Chen et al., 2020; Lepore et al., 2021). As CAPE
 392 is related to the maximum potential updraft within a thunderstorm by $w_{max} = \sqrt{2CAPE}$
 393 (Holton & Hakim, 2013), projections of higher CAPE imply that, on average, future storms
 394 will have stronger updrafts, resulting in deeper, more explosive convection than storms
 395 during the reference period (1971-2000). Additionally, it was shown by Dougherty and
 396 Rasmussen (2021) that updraft intensities increased in flood-producing storms in CONUS

397 simulations, further supporting the hypothesis that increasing CAPE results in an in-
 398 creased risk for severe weather. The spatial patterns in these changes also highlight the
 399 continued influence of the GPLLJ advecting warm, moist air into the Plains and east
 400 of the Rocky Mountains (e.g., Carlson et al., 1983).

401 Epoch differences in boreal spring wind shear reveal a large and spatially coherent
 402 east-west swath of decreasing S06 over the entirety of the CONUS, increasing in mag-
 403 nitude with time in Fig. 5b (Trapp et al., 2007, 2009; Diffenbaugh et al., 2013; Hoogewind
 404 et al., 2017; Lepore et al., 2021; Ting et al., 2019). The greatest changes appear in the
 405 northeast, with smaller decreases over the southern CONUS. Sufficient shear is impera-
 406 tive to the internal dynamics of a thunderstorm since it promotes vertical storm-scale
 407 rotation and assists in sustaining the updraft (Weisman & Rotunno, 2000; Trapp et al.,
 408 2007), which are important ingredients for tornadogenesis, large hail formation, and dam-
 409 aging outflow winds at the surface. Additionally, storm environments characterized by
 410 strong vertical wind shear are more likely to be organized, last longer, and become self-
 411 sustaining systems (e.g., Lilly, 1979; Rotunno, 1981; Klemp, 1987; Weisman & Rotunno,
 412 2000). For these reasons, decreases in shear with time indicate that increasingly fewer
 413 thunderstorms will have the support necessary for the most hazardous and severe storms
 414 to form, including organized mesoscale convective systems (MCS).

415 To further diagnose the projected changes in S06, the changes of zonal and merid-
 416 ional winds near the surface and at 6-km were also analyzed. Future projections of sur-
 417 face winds do not reveal spatially coherent changes over the next century, but the zonal
 418 winds aloft indicate substantial departures from the historical record. In particular, nearly
 419 all of the CESM2-LE members project decreases in upper-level westerly winds over the
 420 CONUS during the boreal spring season that increase in magnitude with time. The causal
 421 mechanisms of these zonal wind changes are being explored further, but preliminary re-
 422 sults suggest a connection to projected future changes in tropical rainfall patterns (not
 423 shown).

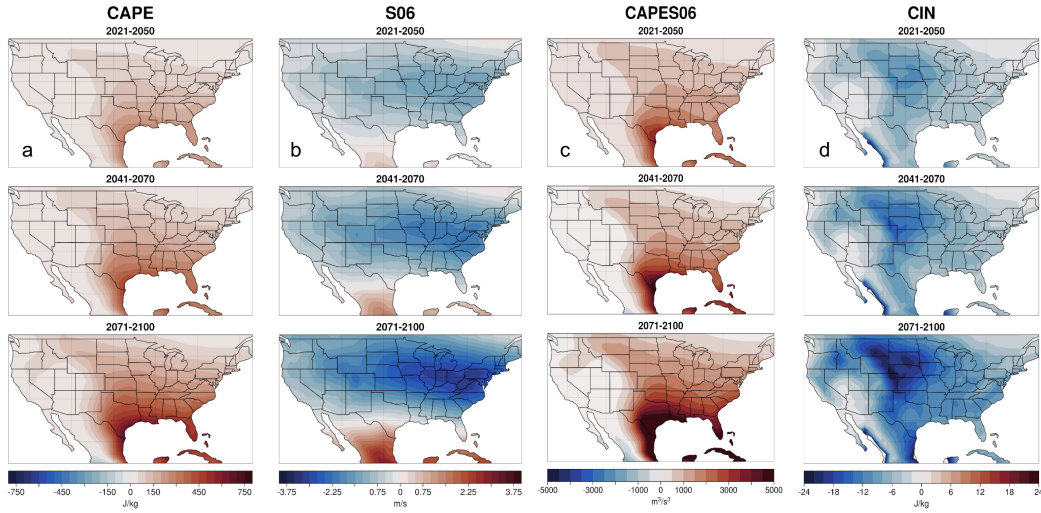


Figure 5. Epoch differences from the 1971-2000 baseline period for early (2021-2050), mid (2041-2070), and end-of-century (2071-2100) convective indices during MAMJ for (a.) CAPE (Jkg^{-1}) (b.) S06 (ms^{-1}) (c.) CAPES06 (m^3s^{-3}) and (d.) CIN (Jkg^{-1})

424 The projected spatial characteristics of changes in CAPES06 (Fig. 5c) are simi-
 425 lar to those highlighted by (Seeley & Romps, 2015), who leveraged four climate mod-

426 els, archived from CMIP5 and forced with two different emission scenarios, to compare
 427 the end-of-century projections of CAPES06 over the U.S. Overall, their findings, as well
 428 as ours, show spatial patterns of boreal spring CAPES06 that are dominated by the changes
 429 in CAPE (Fig. 5a), characterized by a coherent increase with time over the eastern CONUS.
 430 Although the decreases in S06 suggest that there would be less support for storm organ-
 431 ization and dynamics, some studies speculate that the large-scale increases in CAPE will
 432 make up for the diminishing S06 (Trapp et al., 2007, 2009). The main point is that CAPES06
 433 is expected to undergo substantial increases by the end of this century, suggesting con-
 434 vective environments over the southeastern U.S. will be supportive of a higher ratio of
 435 significant severe versus non-severe storms.

436 However, this hypothesis does not take into account the increasing magnitude of
 437 CIN that represents the negative buoyancy that parcels need to overcome in order to re-
 438 alize their CAPE (K. L. Rasmussen et al., 2017). Despite enhanced CAPE values in a
 439 future climate, weak to moderate storms may be less frequent due to enhanced stabil-
 440 ity (i.e. CIN) that requires more lifting or heating to overcome. Changes in the forced
 441 component of CIN projected by the CESM2-LE are characterized by decreases over the
 442 central and northern Great Plains that increase in magnitude throughout this century,
 443 reaching approximately -18 Jkg^{-1} by 2100 (Fig. 5d). Such changes are indicative of a
 444 more stable or “capped” atmosphere. If strong enough ($\text{CIN} < -200 \text{ Jkg}^{-1}$), this stabil-
 445 ity could potentially inhibit convection completely. On the other hand, there is the possi-
 446 bility that there is moderate CIN ($-50 \text{ Jkg}^{-1} > \text{CIN} > -200 \text{ Jkg}^{-1}$), allowing for an ac-
 447 cumulation of CAPE that once released, could produce explosive convection. Globally,
 448 this is commonly observed in convective environments in the vicinity of large mountain
 449 ranges such as the Rockies and the Andes, as discussed in the introduction (Zipser et
 450 al., 2006; K. L. Rasmussen & Houze, 2011; K. L. Rasmussen et al., 2014; K. L. Rasmussen
 451 & Houze, 2016). The juxtaposition of the terrain-induced mid-level capping inversion
 452 with the warm, moist air allows for the modulation of CAPE by CIN until convective
 453 initiation occurs and intense convection is then able to develop. It is also evident in the
 454 spatial patterns (Fig. 5) that by the end of the century, the areas of maximum stabil-
 455 ity are not collocated with the areas of maximum convective energy. Therefore, since CIN
 456 is minimized over the Great Plains, while CAPE is maximized over the eastern U.S., the
 457 future frequency of convection in the Great Plains is, on average, likely to be less than
 458 the current climate but still vigorous due to increased stability, while convective frequency
 459 over the eastern U.S. is likely to be slightly less reduced, but more intense when it does
 460 occur as a result of the increased and accumulated CAPE. Overall, these changes are in
 461 agreement with previous studies using both Earth system models (Hoogewind et al., 2017;
 462 Lepore et al., 2021) and dynamical downscaling or a pseudo-global warming approach,
 463 such as K. L. Rasmussen et al. (2017) and Chen et al. (2020), projecting coherent increases
 464 in the magnitude of CIN over the central and southern Great Plains by 2100 (Fig. 5d).

465 Following the analyses of Brooks et al. (2003), Trapp et al. (2007), and Gensini and
 466 Ashley (2011), the number of days favorable for the formation of severe weather is de-
 467 termined by computing NDSEV. Early-century (2021-2050) changes from the baseline
 468 climatology show an increase in boreal spring NDSEV that is especially pronounced over
 469 the eastern half of the CONUS, with the largest values over the southeastern U.S. (Fig.
 470 6). Increases in NDSEV continue throughout the rest of this century, yielding values more
 471 than double the historical climatology, and largely reflecting spatial patterns evident in
 472 CAPE (Fig. 5a). These findings are further evidence that, by 2100, eastern CONUS will
 473 likely experience an increase in severe storm activity, despite the robust decrease in pro-
 474 jections of S06, especially since the end of century magnitudes of wind shear are still larger
 475 than the severe weather threshold (5 ms^{-1}) (Brooks et al., 2003; Trapp et al., 2007, 2009;
 476 Diffenbaugh et al., 2013; Hoogewind et al., 2017). While the spatial patterns of change
 477 in NDSEV are in broad agreement with previous studies, the magnitude of changes ex-
 478 pected by the end of the century are larger than the aforementioned studies. A detailed
 479 explanation for these differences is beyond the scope of this paper, but it should be noted

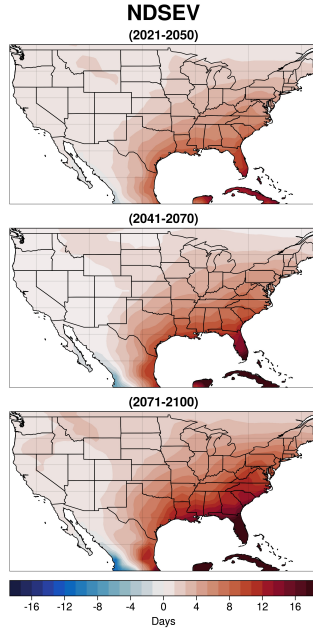


Figure 6. Same as Fig. 5, except for NDSEV (Days).

480 that other studies used slightly different definitions of NDSEV as well as different mod-
 481 els with various forcing scenarios, all of which likely contribute to deviations from the
 482 results shown in Fig. 6.

483 As expressed, the results in this section for CAPE, CIN, S06, and CAPES06 are
 484 all in general agreement with previous literature. What makes this work unique is that
 485 we have been able to show a robust, multi-century estimate of the large-scale convective
 486 environment over the eastern U.S. by using a 50-member ensemble, providing more cer-
 487 tainty in the changes of the forced response due to anthropogenic climate change as sim-
 488 ulated by the CESM2.

489 3.2 Internal Variability

490 Previous studies have primarily focused on changes in convective environments due
 491 to anthropogenic climate change (i.e., the forced response). However, the large ensem-
 492 ble approach provides a novel opportunity to investigate the effect of internal (or unforced)
 493 climate variability and how it might modify the forced response, where all 50 ensemble
 494 members represent an equally possible path to reality. To illustrate the range of possi-
 495 ble outcomes, the simple metric of linear trends for each of the convective indices over
 496 the next 30 years (2021-2050) is considered. Histograms of the ensemble members are
 497 shown in Fig. 7. Changes through 2050 are analyzed because uncertainty due to inter-
 498 nal climate variability is most significant over the next several decades relative to the
 499 forced signal (Hawkins & Sutton, 2009; Deser, 2020).

500 Even in the presence of significant internal variability, 30-year trends of boreal spring
 501 CAPE over the eastern CONUS are positive for all 50 ensemble members (Fig. 7a), but
 502 they exhibit considerable spread. Trends out to 2050 range from near zero to $\sim 68 \text{ Jkg}^{-1}\text{decade}^{-1}$,
 503 while two-thirds of the ensemble members have CAPE trends between 20 and $40 \text{ Jkg}^{-1}\text{decade}^{-1}$.
 504 Similarly, trends in S06 are mostly of the same sign, with 46 of the 50 ensemble mem-
 505 bers exhibiting negative trends with a minimum of $-0.85 \text{ ms}^{-1}\text{decade}^{-1}$ projected by four
 506 members. These results show that the sign of the response of CAPE and S06 to anthro-

507 pogenic forcing (Fig. 4a, b) is robust across nearly all of the CESM2-LE members, but
 508 that the magnitude of the forced response is likely to be considerably moderated by in-
 509 ternal climate variability over the coming decades (Fig. 7a, b). It follows that boreal spring
 510 trends in CAPES06 over the coming decades are positive for nearly all ensemble mem-
 511 bers (Fig. 7c), with 80% of the members exhibiting trends between 100 and 500 $\text{m}^3\text{s}^{-3}\text{decade}^{-1}$.
 512 In contrast, the signs of 30-year trends in boreal spring CIN over the eastern CONUS
 513 are more mixed (Fig. 7d). Twenty-one of the ensemble members exhibit positive trends,
 514 while the other 29 exhibit negative trends down to $-4.25 \text{ Jkg}^{-1}\text{decade}^{-1}$ (Fig. 7d). While
 515 Fig. 4d illustrates a forced decrease in CIN magnitudes by the end of the century, the
 516 robustness of the sign of the change is less certain due to internal climate variability when
 517 averaged over the eastern CONUS (Fig. 7d).

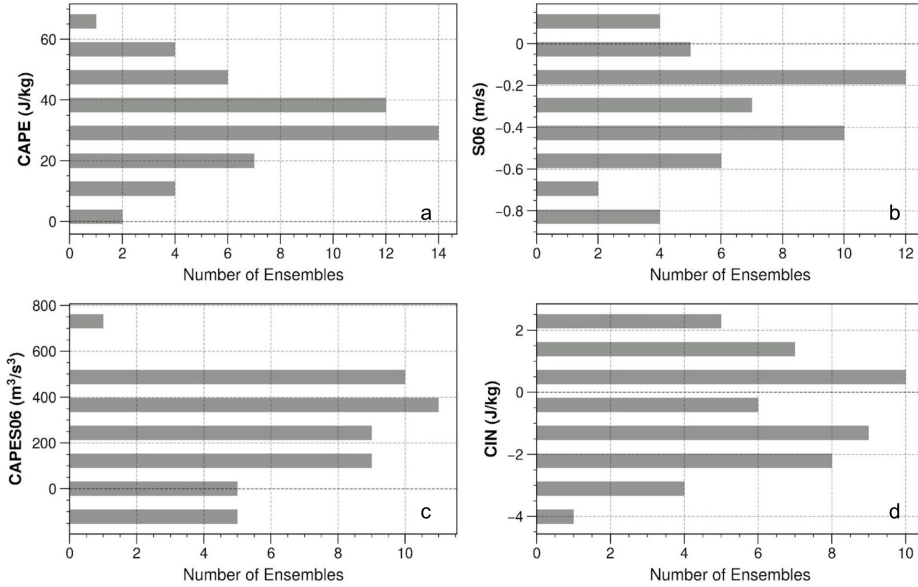


Figure 7. Histograms for 50-member ensemble simulations illustrating the spread of linear trends per decade for the 2021-2050 period during the months March - June for (a.) CAPE ($\text{Jkg}^{-1}\text{decade}^{-1}$) (b.) S06 ($\text{ms}^{-1}\text{decade}^{-1}$) (c.) CAPES06 ($\text{m}^3\text{s}^{-3}\text{decade}^{-1}$) (d.) CIN ($\text{Jkg}^{-1}\text{decade}^{-1}$). Linear trends were calculated using ordinary least squares linear regression and spatial averages were taken over the eastern CONUS region highlighted in Figure 1.

518 To further illustrate the dominant role that internal climate variability is likely to
 519 play over the next several decades, we examine spatial patterns of change by selecting
 520 the ensemble members with the largest and smallest trends in area-averaged convective
 521 indices over the eastern CONUS during the boreal spring seen in Fig. 7. CAPES06 is
 522 discussed since it considers two of the most important elements necessary for severe weather:
 523 the thermodynamic energy and kinematic support (Fig. 8).

524 Ensemble member 25 exhibits the most negative (minimum) CAPES06 trend (-182
 525 $\text{Jkg}^{-1}\text{decade}^{-1}$) when averaged over the eastern CONUS, while ensemble member 23 has
 526 the largest trend ($791 \text{ Jkg}^{-1}\text{decade}^{-1}$) (Fig. 7c). The spatial patterns of the linear decadal
 527 trends in CAPES06 for these two simulations are shown in Fig. (8a, d), respectively. By
 528 removing the forced trend (ensemble-mean) from each of these individual ensemble mem-
 529 bers (Fig. 8b, e), the changes in CAPES06 over the next several decades due purely to
 530 internal variability are revealed (Fig. 8c, f). In general, the signals of internal climate

531 variability are spatially coherent and are of a larger magnitude over the next several decades
 532 than the forced trends. In ensemble member 25, internal climate variability counteracts
 533 the forced, positive change in CAPES06 over much of the southeastern U.S. (Fig. 8c),
 534 resulting in an overall negative trend over much of the region (Fig. 8a). Conversely, in
 535 ensemble member 23, internal climate variability (Fig. 8f) augments the forced signal
 536 and produces a very strong increase through 2050, especially over parts of Texas and the
 537 southern Great Plains (Fig. 8d). These two ensemble members were subjectively selected
 538 to most dramatically illustrate the role of internal climate variability in modulating the
 539 forced response in CAPES06, but a similar approach can be taken with the other ensem-
 540 ble members in Fig. 7 to illustrate the large-scale, coherent spatial patterns of internal
 541 variability that significantly modify the forced trend.

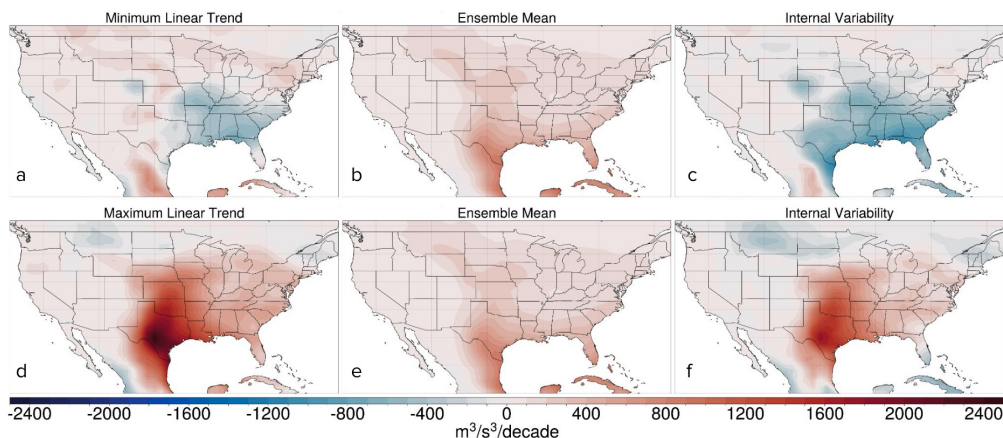


Figure 8. Linear decadal trends for 2021-2050 over the eastern CONUS for the ensemble numbers 25 (top row) and 23 (bottom row) for the full (left; a, d), forced (middle; b, e), and internal (right; c, f) components of MAMJ CAPES06 ($\text{m}^3\text{s}^{-3}\text{decade}^{-1}$).

542 Similarly, the dominant role of internal variability in affecting NDSEV is illustrated
 543 in Fig. 9. On average, over the next several decades (2021-2050), anthropogenic climate
 544 change is likely to increase the number of days in boreal spring with convective environ-
 545 ments favorable for the development of severe weather over most of the CONUS, with
 546 the largest increases over the southeastern U.S. (Fig. 9b, 9e). However, as shown by en-
 547 semble member 41 (Fig. 9a), a plausible outcome by 2050 is that internal climate vari-
 548 ability could substantially reduce the number of days favorable for severe weather (Fig.
 549 9c). Conversely, ensemble member 23 shows that internal climate variability (Fig. 9f)
 550 could augment the increases from climate change, resulting in a large increase in ND-
 551 SEV by 2050 (Fig. 9d). While internal fluctuations may be considered to be inherently
 552 chaotic and random, they are a product of the large-scale dynamics and thus, are spa-
 553 tially coherent with relatively large magnitudes (Fig. 8, 9). Further examining the cir-
 554 culation anomalies that drive such internal variations in these convective parameters is
 555 the subject of future work. A key point is that when considering future projections of
 556 greenhouse-gas forced changes in severe weather environments, the extent to which they
 557 will be modulated by internal variability is important to consider.

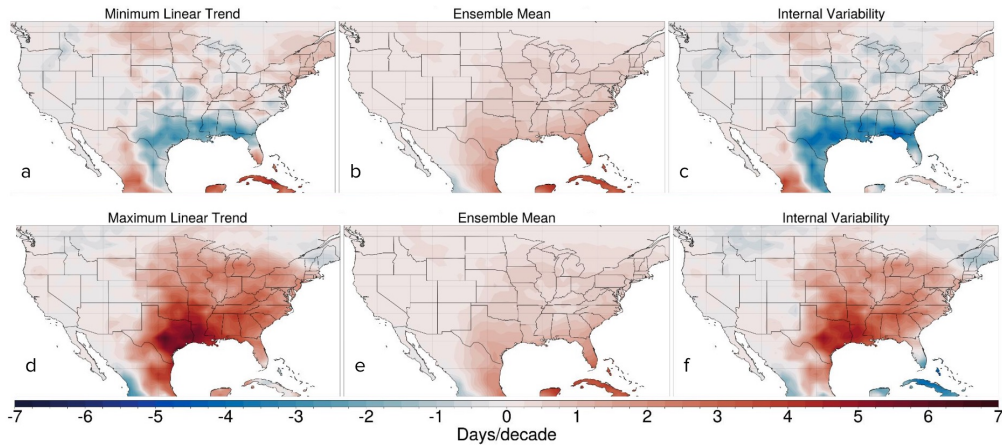


Figure 9. Linear decadal trends for 2021-2050 over the eastern CONUS for the ensemble numbers 41 (top row) and 23 (bottom row) for the full (left; a, d), forced (middle; b, e), and internal (right; c, f) components of MAMJ NDSEV (Daysdecade^{-1}).

558 In addition to employing covariate proxies, epoch bivariate distribution plots, or
 559 two-dimensional histograms, were created to examine the future phase spaces (i.e., con-
 560 vective frequency and intensity) of various convective indices, due to both forced and in-
 561 ternal variability, to gain more insight into changes in the convective mode. As mentioned
 562 earlier, K. L. Rasmussen et al. (2017) used dynamical downscaling to produce convection-
 563 permitting regional climate model projections of end-of-century (2071-2100) May-June
 564 CAPE and CIN over the Midwest to examine changes in the thermodynamic environ-
 565 ment. By producing a two-dimensional histogram, they found that by the end of the cen-
 566 tury, convective environments are increasingly characterized by higher average CAPE
 567 ($\sim 400 \text{ Jkg}^{-1}$) and lower average (or increased) CIN ($\sim -80 \text{ Jkg}^{-1}$) indicative of more
 568 vigorous convective storms but a stronger capping inversion. We have taken a similar
 569 approach using the CESM2-LE to illustrate changes in both the forced and internal com-
 570 ponents of the convective indices over time. The bivariate distributions of the histor-
 571 ical climatology (1971-2000, blue) and future 30-year periods (2021-2050, orange; and 2071-
 572 2100, green) are shown in Fig. 10. Individual, or marginal, distributions are displayed
 573 on the opposite axis for each index, helping to highlight the range due to internal vari-
 574 ability, and how it changes through the century. While the shape of the distribution gives
 575 some insight into the range of internal variability, the shifts in the CAPE versus CIN pat-
 576 tern as a whole are due to the changes over time in the forced response.

577 For the late 20th century (blue), the distribution in Fig. 10a has the highest den-
 578 sity of ensemble members around CAPE values of 440 Jkg^{-1} and CIN values around -29 Jkg^{-1} .
 579 Over the next several decades (orange), the distribution exhibits an overall
 580 shift toward the bottom right of the diagram with relatively higher CAPE (560 Jkg^{-1})
 581 and relatively lower, or increased magnitudes, of CIN (-36 Jkg^{-1}). By the end of the 21st
 582 century (green), the CAPE versus CIN distribution has shifted to even higher CAPE and
 583 lower CIN, with average magnitudes of $\sim 745 \text{ Jkg}^{-1}$ and -40 Jkg^{-1} , respectively (Fig.
 584 10a). In Fig. 10a, the shape of the end-of-century epoch (green) indicates that the fu-
 585 ture projections of CAPE could be anywhere from approximately 500 to 1050 Jkg^{-1} by
 586 the end of the century. Conversely, even with an ensemble mode of -40 Jkg^{-1} , the range
 587 of future projections for CIN due to the internal variability could fall anywhere between
 588 -26 and -70 Jkg^{-1} (Fig. 10a). Thus, even though a wide range of plausible outcomes ex-
 589 ist for both CAPE and CIN due to the role of internal variability, a majority of the en-
 590 semble members suggest future environments over the southeastern CONUS will be com-

591 posed of higher CAPE and increased magnitudes of CIN compared to the present-day
 592 climate (Diffenbaugh et al., 2013; K. L. Rasmussen et al., 2017; Lepore et al., 2021). The
 593 balance between these two thermodynamic indices is key to determining future convective
 594 modes and frequency (Diffenbaugh et al., 2013; K. L. Rasmussen et al., 2017; Chen
 595 et al., 2020; Lepore et al., 2021).

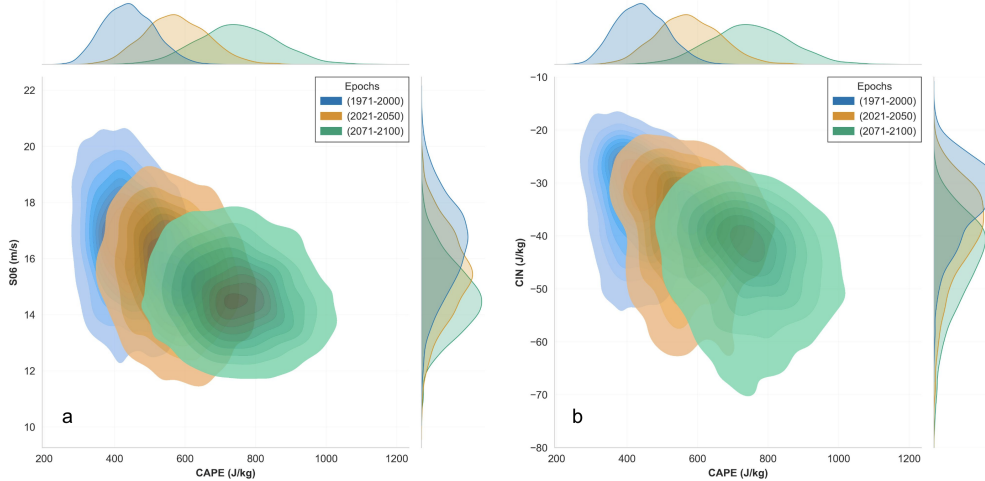


Figure 10. Bivariate distributions over eastern CONUS for MAMJ (a.) CAPE (Jkg^{-1}) vs. CIN (Jkg^{-1}) and (b.) CAPE (Jkg^{-1}) vs. S06 (ms^{-1}) for various epochs: 1971-2000 in blue, 2021-2050 in orange, and 2071-2100 in green. Marginal distributions for each index and period are shown on the opposite axis.

596 The same analysis can be done for the CAPE and vertical wind shear phase space
 597 (Fig. 10b), which is key for storm type and organization. Overall, the phase space of these
 598 two indices shifts from relatively moderate CAPE and high S06 to higher CAPE and lower
 599 S06 (Trapp et al., 2007; Diffenbaugh et al., 2013; Hoogewind et al., 2017; Lepore et al.,
 600 2021). The CAPE distributions are the same as Fig. 10a, but the distribution in bulk
 601 vertical wind shear follows a decreasing trend throughout the century, with an ensemble
 602 mode of approximately 14.5 ms^{-1} by 2100 (Fig. 10b, green). It is also clear that, from
 603 the historical climatology to the end of the century, the shapes of the epochs evolve from
 604 long and narrow to a more circular shape. In other words, the uncertainty in S06 changes
 605 due to internal variability is likely to decrease as the century progresses, whereas the un-
 606 certainty in changes to CAPE is likely to increase. Previously, Brooks et al. (2003) an-
 607 alyzed soundings from reanalysis data that were associated with severe thunderstorms
 608 in the U.S. from 1997-1999. These soundings were further classified as little severe, sig-
 609 nificant severe, and significant tornadoes. Their two-dimensional histogram of CAPE and
 610 S06 indicated the most severe storms were characterized by high CAPE and high wind
 611 shear (i.e., the top right of Fig. 10b). Further, the storms that were classified as sig-
 612 nificant tornadoes had S06 greater than 10 ms^{-1} , and storms that were classified as sig-
 613 nificant severe exhibited S06 greater than 5 ms^{-1} . The distribution for significant severe
 614 storms existed over the high CAPE region ($100\text{-}5000 \text{ Jkg}^{-1}$), but significant tornadoes
 615 exhibited values across the full range of CAPE distributions.

616 Comparing our results to the storm classifications in Brooks et al. (2003) and other
 617 studies (E. N. Rasmussen & Blanchard, 1998; Brooks, 2009), the projected increases in
 618 end-of-century CAPE will be more than sufficient to support significant severe storms
 619 and tornadoes. Although, while S06 is projected to decrease, even in the presence of in-

620 ternal variability, the absolute magnitudes of wind shear (Fig. 10b) remain above the
 621 threshold to produce significant severe weather, but may not be as supportive of the most
 622 intense types of severe weather (e.g. tornadoes or derechos). The implication of higher
 623 CAPE and lower S06 is that when future storms do occur, there is a smaller chance that
 624 they will have the necessary dynamical support and organization to produce the most
 625 intense severe weather compared to the current climate, paralleling past research (Difffenbaugh
 626 et al., 2013; Lepore et al., 2021).

627 4 Discussion and Conclusion

628 An important goal of this study was to better understand how severe and hazardous
 629 weather is likely to change in a warmer, future climate. While the spatiotemporal scales
 630 on which severe storms form are smaller than can be explicitly resolved by relatively coarse
 631 resolution models such as the CESM2, such models can be leveraged to instead exam-
 632 ine the evolution of the large-scale convective environments in which the storms develop.
 633 Further, by using a large ensemble of climate model simulations as we have done with
 634 the CESM2-LE, it is possible to not only identify and examine anthropogenically-forced
 635 changes in convective environments over time but also how the forced changes are likely
 636 to be altered by internal climate variability. This latter aspect, to our knowledge, has
 637 yet to be robustly documented. An increased understanding of the range of plausible,
 638 future convective environments can enhance our capability to better project the nature
 639 of severe weather in the future, and perhaps increase resilience to these hazards.

640 Our study is novel in that we have examined the continuous-time evolution of var-
 641 ious convective indices from 1870-2100 over the CONUS using a 50-member ensemble
 642 from a well-documented and understood Earth system model. By using a large ensem-
 643 ble from a single model, we were able to obtain a robust estimate of the forced response.
 644 Our results are in agreement with previous studies that anthropogenic climate change
 645 will likely drive future convective environments over the eastern U.S. toward less frequent,
 646 but more intense and deep convection. Additionally, there will also be less kinematic sup-
 647 port, which means less support for the organization of supercells and other multi-cellular
 648 convective storm modes capable of delivering the most extreme severe weather risks.

649 By taking advantage of a large ensemble approach, this study was further able to
 650 robustly investigate the effect of internal climate variability on large-scale convective en-
 651 vironments, rather than just the forced response as most previous studies have done. While
 652 we have shown that the end-of-century changes in convective environments due to the
 653 forced response are spatially coherent and robust, we have also demonstrated how these
 654 changes can be substantially modulated by internal variability. The latter has spatial
 655 coherency and thus can either significantly enhance or suppress the forced changes.

656 Examining the convective proxies and the bivariate distributions of the selected in-
 657 dices, it is likely that future environments will be characterized by higher CAPE, moderate-
 658 high magnitudes of CIN, and lower S06, which is in general agreement with previous lit-
 659 erature. Our results thus suggest that there will be an increase in frequency in the less
 660 severe convective modes such as multi-cellular and ordinary thunderstorms. The actual
 661 time evolution of these quantities will, of course, not only be influenced by forced climate
 662 change, but also by internal variability. While it is not possible to make a determinis-
 663 tic prediction of how actual convective environments over the CONUS will evolve through-
 664 out the rest of this century, our study has helped to quantify the range of uncertainty
 665 and plausible scenarios.

666 Our conclusions depend on the assumption that the CESM2-LE is capable of ac-
 667 curately simulating the future, even though it performs well in simulating past convective
 668 environments (e.g., Figs. 2, 3). Our results are also dependent on the future forc-
 669 ing scenario (SSP3-7.0) used to produce the CESM2-LE.

This study is the first to exploit the CESM2-LE to examine changes in convective parameters. Plans for future work include more comprehensive regional analyses, especially since some regions are less influenced by internal variability than others (Deser et al., 2012b), and in this study, averages have been taken over a very large spatial domain (Fig. 1). Also, given the prominent and coherent role of internal variability over the southeastern U.S., further analysis is necessary to examine the large-scale circulation changes that drive internal variations in the convective indices, and if those circulation changes are connected to large-scale coupled modes of climate variability. If so, it will be important to determine the level of predictability associated with internal variability. Finally, similar analyses for other seasons, as well as other regions of the world where convective activity is pronounced, such as over Argentina on the lee-side of the Andes (e.g., Zipser et al., 2006; K. L. Rasmussen & Houze, 2011; K. L. Rasmussen et al., 2014; Mulholland et al., 2018; Nesbitt et al., 2021) are underway. A better understanding of the possible future evolution and variability in large-scale convective environments is critical for understanding future changes in severe weather hazards and in particular, how we choose to adapt to these hazards.

Open Research Section

The first 50 ensemble members from The Community Earth System Model Version 2-Large Ensemble data (CESM2-LE; Danabasoglu et al., 2020; Rodgers et al., 2021) used for this study can be found and downloaded publicly online at <https://doi.org/10.26024/kgmp-c556>. Data from the Fifth-Generation Global Climate Reanalysis (ERA5; Hersbach et al., 2020) can also be found and downloaded publicly online at <https://doi.org/10.5065/BH6N-5N20>.

Acknowledgments

We would like to acknowledge the CESM2 Large Ensemble Community Project and supercomputing resources provided by the IBS Center for Climate Physics in South Korea. In addition, we would also like to acknowledge Dan Chavas of Purdue University for preliminary conversations regarding this project, as well as for providing us with the calculated ERA5 convective parameters used in this study. Thank you to the listed co-authors for their support and guidance in completing this project as well as to the Department of Atmospheric Science and the Walter Scott, Jr. College of Engineering at Colorado State University.

References

- Allen, J. T., Tippett, M. K., & Sobel, A. H. (2015). Influence of the El Niño/Southern Oscillation on tornado and hail frequency in the United States. *Nature Geoscience*, *8*(4), 278–283. doi: 10.1038/ngeo2385
- Brooks, H. E. (2009). Proximity soundings for severe convection for Europe and the United States from reanalysis data. *Atmospheric Research*, *93*, 546–553. doi: 10.1016/j.atmosres.2008.10.005
- Brooks, H. E., Lee, J. W., & Craven, J. P. (2003). The spatial distribution of severe thunderstorm and tornado environments from global reanalysis data. *Atmospheric Research*, *67-68*, 73–94. doi: 10.1016/S0169-8095(03)00045-0
- Capotondi, A., Deser, C., Phillips, A. S., Okumura, Y., & Larson, S. M. (2020). ENSO and Pacific Decadal Variability in the Community Earth System Model Version 2. *Journal of Advances in Modeling Earth Systems*, *12*(12), e2019MS002022. doi: 10.1029/2019MS002022
- Carlson, T. N., Benjamin, S. G., Forbes, G. S., & Li, Y.-F. (1983). Elevated Mixed Layers in the Regional Severe Storm Environment: Conceptual Model and Case Studies. *Monthly Weather Review*, *111*(7), 1453–1474. doi:

- 10.1175/1520-0493(1983)111<1453:EMLITR>2.0.CO;2
- 719
720 Chen, J., Dai, A., Zhang, Y., & Rasmussen, K. L. (2020). Changes in Convective
721 Available Potential Energy and Convective Inhibition under Global Warming.
722 *Journal of Climate*, *33*(6), 2025–2050. doi: 10.1175/JCLI-D-19-0461.1
- 723 Colby, F. P. (1984). Convective Inhibition as a Predictor of Convection during AVE-
724 SESAME II. *Monthly Weather Review*, *112*(11), 2239–2252. doi: 10.1175/1520-
725 -0493(1984)112<2239:CIAAPO>2.0.CO;2
- 726 Craven, J. P., & Brooks, H. E. (2004). Baseline Climatology of Sounding Derived
727 Parameters Associated With Deep Moist Convection. *National Weather Di-
728 gest*, *28*, 13–24. [https://www.nssl.noaa.gov/users/brooks/public.html/
729 papers/cravenbrooksna.pdf](https://www.nssl.noaa.gov/users/brooks/public.html/papers/cravenbrooksna.pdf).
- 730 Craven, J. P., Jewell, R. E., & Brooks, H. E. (2002). Comparison between Ob-
731 served Convective Cloud-Base Heights and Lifting Condensation Level for
732 Two Different Lifted Parcels. *Weather and Forecasting*, *17*(4), 885–890. doi:
733 10.1175/1520-0434(2002)017<0885:CBOCCB>2.0.CO;2
- 734 Dai, A., Fung, I. Y., & Genio, A. D. D. (1997). Surface Observed Global Land Pre-
735 cipitation Variations during 1900–88. *Journal of Climate*, *10*(11), 2943–2962.
736 doi: 10.1175/1520-0442(1997)010<2943:SOGLPV>2.0.CO;2
- 737 Dai, A., & Wigley, T. M. L. (2000). Global patterns of ENSO-induced precipitation.
738 *Geophysical Research Letters*, *27*(9), 1283–1286. doi: 10.1029/1999GL011140
- 739 Danabasoglu, G., Lamarque, J.-F., Bacmeister, J., Bailey, D. A., DuVivier, A. K.,
740 Edwards, J., et al. (2020). The Community Earth System Model Ver-
741 sion 2 (CESM2). *Journal of Advances in Modeling Earth Systems*, *12*(2),
742 e2019MS001916. doi: 10.1029/2019MS001916
- 743 Deser, C. (2020). “Certain Uncertainty: The Role of Internal Climate Variability in
744 Projections of Regional Climate Change and Risk Management”. *Earth’s Fu-
745 ture*, *8*(12), e2020EF001854. doi: 10.1029/2020EF001854
- 746 Deser, C., Knutti, R., Solomon, S., & Phillips, A. S. (2012b). Communication of the
747 role of natural variability in future North American climate. *Nature Climate
748 Change*, *2*(11). doi: 10.1038/nclimate1562
- 749 Deser, C., Phillips, A., Bourdette, V., & Teng, H. (2012a). Uncertainty in climate
750 change projections: the role of internal variability. *Climate Dynamics*, *38*(3),
751 527–546. doi: 10.1007/s00382-010-0977-x
- 752 Diffenbaugh, N. S., Scherer, M., & Trapp, R. J. (2013). Robust increases in severe
753 thunderstorm environments in response to greenhouse forcing. *Proceedings of
754 the National Academy of Sciences*, *110*(41), 16361–16366. doi: 10.1073/pnas
755 .1307758110
- 756 Doswell, C. A., & Rasmussen, E. N. (1994). The Effect of Neglecting the Virtual
757 Temperature Correction on CAPE Calculations. *Weather and Forecasting*,
758 *9*(4), 625–629. doi: 10.1175/1520-0434(1994)009<0625:TEONTV>2.0.CO;2
- 759 Dougherty, E., & Rasmussen, K. L. (2021). Variations in Flash Flood-Producing
760 Storm Characteristics Associated with Changes in Vertical Velocity in a Future
761 Climate in the Mississippi River Basin. *Journal of Hydrometeorology*, *22*(3),
762 671–687. doi: 10.1175/JHM-D-20-0254.1
- 763 Eyring, V., Bony, S., Meehl, G. A., Senior, C. A., Stevens, B., Stouffer, R. J., &
764 Taylor, K. E. (2016). Overview of the Coupled Model Intercomparison Project
765 Phase 6 (CMIP6) experimental design and organization. *Geoscientific Model
766 Development*, *9*(5), 1937–1958. doi: 10.5194/gmd-9-1937-2016
- 767 Gensini, V. A., & Ashley, W. S. (2011). Climatology of Potentially Severe Convec-
768 tive Environments from the North American Regional Reanalysis. *Electronic J.
769 Severe Storms Meteor*, *6*(8), 1–40. doi: 10.55599/ejssm.v6i8.35
- 770 Gettelman, A., & Morrison, H. (2015). Advanced Two-Moment Bulk Micro-
771 physics for Global Models. Part I: Off-Line Tests and Comparison with
772 Other Schemes. *Journal of Climate*, *28*(3), 1268–1287. doi: 10.1175/
773 JCLI-D-14-00102.1

- 774 Golaz, J.-C., Larson, V. E., & Cotton, W. R. (2002). A PDF-Based Model for
775 Boundary Layer Clouds. Part I: Method and Model Description. *Journal of*
776 *the Atmospheric Sciences*, *59*(24), 3540–3551. doi: 10.1175/1520-0469(2002)
777 059(3540:APBMFB)2.0.CO;2
- 778 Hawkins, E., & Sutton, R. (2009). The Potential to Narrow Uncertainty in Regional
779 Climate Predictions. *Bulletin of the American Meteorological Society*, *90*(8),
780 1095–1108. doi: 10.1175/2009BAMS2607.1
- 781 Hersbach, H., Bell, B., Berrisford, P., Hirahara, S., Horányi, A., Muñoz-Sabater, J.,
782 ... Thépaut, J.-N. (2020). The ERA5 global reanalysis. *Quarterly Journal of*
783 *the Royal Meteorological Society*, *146*(730), 1999–2049. doi: 10.1002/qj.3803
- 784 Higgins, R. W., Yao, Y., Yarosh, E. S., Janowiak, J. E., & Mo, K. C. (1997). In-
785 fluence of the Great Plains Low-Level Jet on Summertime Precipitation and
786 Moisture Transport over the Central United States. *Journal of Climate*, *10*(3),
787 481–507. doi: 10.1175/1520-0442(1997)010(0481:IOTGPL)2.0.CO;2
- 788 Holton, J. R., & Hakim, G. J. (2013). Chapter 9 - Mesoscale Circulations. In *An In-*
789 *troduction to Dynamic Meteorology* (Fifth ed., p. 279-323). Boston: Academic
790 Press. doi: 10.1016/B978-0-12-384866-6.00009-X
- 791 Hoogewind, K. A., Baldwin, M. E., & Trapp, R. J. (2017). The Impact of Cli-
792 mate Change on Hazardous Convective Weather in the United States: Insight
793 from High-Resolution Dynamical Downscaling. *Journal of Climate*, *30*(24),
794 10081–10100. doi: 10.1175/JCLI-D-16-0885.1
- 795 Hurrell, J. W., Holland, M. M., Gent, P. R., Ghan, S., Kay, J. E., Kushner, P. J.,
796 ... Marshall, S. (2013). The Community Earth System Model: A Framework
797 for Collaborative Research. *Bulletin of the American Meteorological Society*,
798 *94*(9), 1339–1360. doi: 10.1175/BAMS-D-12-00121.1
- 799 IPCC. (2021). Summary for policymakers. In *Climate Change 2021: The Physical*
800 *Science Basis. Contribution of Working Group I to the Sixth Assessment Re-*
801 *port of the Intergovernmental Panel on Climate Change* (p. 332). Cambridge,
802 United Kingdom and New York, NY, USA: Cambridge University Press. doi:
803 10.1017/9781009157896.001
- 804 Johns, R. H., & Doswell, C. A. (1992). Severe Local Storms Forecasting. *Weather*
805 *and Forecasting*, *7*(4), 588–612. doi: 10.1175/1520-0434(1992)007(0588:SLSF)2
806 .0.CO;2
- 807 Kelly, D. L., Schaefer, J. T., & Doswell, C. A. (1985). Climatology of Nontornadic
808 Severe Thunderstorm Events in the United States. *Monthly Weather Review*,
809 *113*(11), 1997–2014. doi: 10.1175/1520-0493(1985)113(1997:CONSTE)2.0.CO;
810 2
- 811 Kirtman, B. P., Min, D., Infanti, J. M., Kinter, J. L., Paolino, D. A., Zhang, Q., ...
812 Wood, E. F. (2014). The North American Multimodel Ensemble: Phase-1
813 Seasonal-to-Interannual Prediction; Phase-2 toward Developing Intraseasonal
814 Prediction. *Bulletin of the American Meteorological Society*, *95*(4), 585–601.
815 doi: 10.1175/BAMS-D-12-00050.1
- 816 Klemp, J. B. (1987). Dynamics of Tornadic Thunderstorms. *Annual Review of Fluid*
817 *Mechanics*, *19*(1), 369–402. doi: 10.1146/annurev.fl.19.010187.002101
- 818 Lee, S.-K., Atlas, R., Enfield, D., Wang, C., & Liu, H. (2013). Is There an Optimal
819 ENSO Pattern That Enhances Large-Scale Atmospheric Processes Conducive
820 to Tornado Outbreaks in the United States? *Journal of Climate*, *26*(5), 1626–
821 1642. doi: 10.1175/JCLI-D-12-00128.1
- 822 Lepore, C., Abernathy, R., Henderson, N., Allen, J. T., & Tippett, M. K. (2021).
823 Future Global Convective Environments in CMIP6 Models. *Earth's Future*,
824 *9*(12), e2021EF002277. doi: 10.1029/2021EF002277
- 825 Li, F., Chavas, D. R., Reed, K. A., & Dawson II, D. T. (2020). Climatology of
826 Severe Local Storm Environments and Synoptic-Scale Features over North
827 America in ERA5 Reanalysis and CAM6 Simulation. *Journal of Climate*,
828 *33*(19), 8339–8365. doi: 10.1175/JCLI-D-19-0986.1

- 829 Li, W., Li, L., Fu, R., Deng, Y., & Wang, H. (2011). Changes to the North At-
 830 lantic Subtropical High and Its Role in the Intensification of Summer Rainfall
 831 Variability in the Southeastern United States. *Journal of Climate*, *24*(5),
 832 1499–1506. doi: 10.1175/2010JCLI3829.1
- 833 Lilly, D. K. (1979). The Dynamical Structure and Evolution of Thunderstorms and
 834 Squall Lines. *Annual Review of Earth and Planetary Sciences*, *7*, 117. doi: 10
 835 .1146/annurev.ea.07.050179.001001
- 836 Liu, C., Ikeda, K., Rasmussen, R., Barlage, M., Newman, A. J., Prein, A. F., ...
 837 Yates, D. (2017). Continental-scale convection-permitting modeling of the cur-
 838 rent and future climate of North America. *Climate Dynamics*, *49*(1), 71–95.
 839 doi: 10.1007/s00382-016-3327-9
- 840 Ludlam, F. H. (1963). Severe Local Storms: A Review. In *Severe Local Storms*
 841 *Meteorological Monographs* (Vol. 5, pp. 1–32). American Meteorological Soci-
 842 ety. doi: 10.1007/978-1-940033-56-3.1
- 843 Mankin, J. S., Lehner, F., Coats, S., & McKinnon, K. A. (2020). The Value of
 844 Initial Condition Large Ensembles to Robust Adaptation Decision-Making.
 845 *Earth's Future*, *8*(10). doi: 10.1029/2020EF001610
- 846 Milinski, S., Maher, N., & Olonscheck, D. (2020). How large does a large ensemble
 847 need to be? *Earth System Dynamics*, *11*(4), 885–901. doi: 10.5194/esd-11-885
 848 -2020
- 849 Mulholland, J. P., Nesbitt, S. W., Trapp, R. J., Rasmussen, K. L., & Salio, P. V.
 850 (2018). Convective Storm Life Cycle and Environments near the Sierras de
 851 Córdoba, Argentina. *Monthly Weather Review*, *146*(8), 2541–2557. doi:
 852 10.1175/MWR-D-18-0081.1
- 853 NCEI. (2021). NOAA National Centers for Environmental Information (NCEI) U.S.
 854 Billion-Dollar Weather and Climate Disasters.
 855 doi: 10.25921/stkw-7w73
- 856 Neale, R. B., & Gettelman, A. (2012). Description of the NCAR Community Atmo-
 857 sphere Model (CAM 5.0) (No. NCAR/TN-486+STR). University Corporation
 858 for Atmospheric Research.
 859 doi: 10.5065/wgtk-4g06
- 860 Nesbitt, S. W., Salio, P. V., Ávila, E., Bitzer, P., Carey, L., Chandrasekar, V., ...
 861 Grover, M. A. (2021). A Storm Safari in Subtropical South America: Proyecto
 862 RELAMPAGO. *Bulletin of the American Meteorological Society*, *102*(8),
 863 E1621–E1644. doi: 10.1175/BAMS-D-20-0029.1
- 864 O'Neill, B. C., Tebaldi, C., van Vuuren, D. P., Eyring, V., Friedlingstein, P., Hurtt,
 865 G., ... Sanderson, B. M. (2016). The Scenario Model Intercomparison Project
 866 (ScenarioMIP) for CMIP6. *Geoscientific Model Development*, *9*(9), 3461–3482.
 867 doi: 10.5194/gmd-9-3461-2016
- 868 Otto-Bliesner, B. L., Brady, E. C., Fasullo, J., Jahn, A., Landrum, L., Steven-
 869 son, S., ... Strand, G. (2016). Climate Variability and Change since 850
 870 CE: An Ensemble Approach with the Community Earth System Model.
 871 *Bulletin of the American Meteorological Society*, *97*(5), 735–754. doi:
 872 10.1175/BAMS-D-14-00233.1
- 873 Pitchford, K. L., & London, J. (1962). The Low-Level Jet as Related to Nocturnal
 874 Thunderstorms over Midwest United States. *Journal of Applied Meteorol-
 875 ogy and Climatology*, *1*(1), 43–47. doi: 10.1175/1520-0450(1962)001<0043:
 876 TLLJAR>2.0.CO;2
- 877 Rasmussen, E. N., & Blanchard, D. O. (1998). A Baseline Climatology of Sounding-
 878 Derived Supercell and Tornado Forecast Parameters. *Weather and Forecasting*,
 879 *13*(4), 1148–1164. doi: 10.1175/1520-0434(1998)013<1148:ABCOSD>2.0.CO;2
- 880 Rasmussen, K. L., & Houze, R. A. (2011). Orographic Convection in Subtropical
 881 South America as Seen by the TRMM Satellite. *Monthly Weather Review*,
 882 *139*(8), 2399–2420. doi: 10.1175/MWR-D-10-05006.1

- 883 Rasmussen, K. L., & Houze, R. A. (2016). Convective Initiation near the Andes in
 884 Subtropical South America. *Monthly Weather Review*, *144*(6), 2351–2374. doi:
 885 10.1175/MWR-D-15-0058.1
- 886 Rasmussen, K. L., Prein, A. F., Rasmussen, R. M., Ikeda, K., & Liu, C. (2017).
 887 Changes in the convective population and thermodynamic environments in
 888 convection-permitting regional climate simulations over the United States.
 889 *Climate Dynamics*, *55*(1), 383–408. doi: 10.1007/s00382-017-4000-7
- 890 Rasmussen, K. L., Zuluaga, M. D., & Houze Jr., R. A. (2014). Severe convection and
 891 lightning in subtropical south america. *Geophysical Research Letters*, *41*(20),
 892 7359–7366. doi: 10.1002/2014GL061767
- 893 Riemann-Campe, K., Fraedrich, K., & Lunkeit, F. (2009). Global climatology of
 894 Convective Available Potential Energy (CAPE) and Convective Inhibition
 895 (CIN) in ERA-40 reanalysis. *Atmospheric Research*, *93*(1), 534–545. doi:
 896 10.1016/j.atmosres.2008.09.037
- 897 Rochette, S. M., Moore, J. T., & Market, P. S. (1999). The importance of parcel
 898 choice in elevated CAPE computations. *Natl. Wea. Dig*, *23*(4), 20–32.
- 899 Rodgers, K. B., Lee, S.-S., Rosenbloom, N., Timmermann, A., Danabasoglu,
 900 G., Deser, C., et al. (2021). Ubiquity of human-induced changes in
 901 climate variability. *Earth System Dynamics*, *12*(4), 1393–1411. doi:
 902 10.5194/esd-12-1393-2021
- 903 Ropelewski, C. F., & Halpert, M. S. (1986). North American Precipitation
 904 and Temperature Patterns Associated with the El Niño/Southern Oscil-
 905 lation (ENSO). *Monthly Weather Review*, *114*(12), 2352–2362. doi:
 906 10.1175/1520-0493(1986)114<2352:NAPATP>2.0.CO;2
- 907 Rotunno, R. (1981). On the Evolution of Thunderstorm Rotation. *Monthly Weather*
 908 *Review*, *109*(3), 577–586. doi: 10.1175/1520-0493(1981)109<0577:OTEOTR>2.0
 909 .CO;2
- 910 Rotunno, R., Klemp, J. B., & Weisman, M. L. (1988). A Theory for Strong, Long-
 911 Lived Squall Lines. *Journal of the Atmospheric Sciences*, *45*(3), 463–485. doi:
 912 10.1175/1520-0469(1988)045<0463:ATFSL>2.0.CO;2
- 913 Seeley, J. T., & Romps, D. M. (2015). The Effect of Global Warming on Severe
 914 Thunderstorms in the United States. *Journal of Climate*, *28*(6), 2443–2458.
 915 doi: 10.1175/JCLI-D-14-00382.1
- 916 Skamarock, W. C., Klemp, J. B., Dudhia, J., Gill, D. O., Barker, D. M., Duda,
 917 M. G., ... Powers, J. G. (2008). A Description of the Advanced Research
 918 WRF Version 3 (No. NCAR/TN-475+STR). University Corporation for Atmo-
 919 spheric Research.
 920 doi: 10.5065/D68S4MVH
- 921 Taszarek, M., Allen, J. T., Marchio, M., & Brooks, H. E. (2021). Global climatology
 922 and trends in convective environments from ERA5 and rawinsonde data. *npj*
 923 *Climate and Atmospheric Science*, *4*(1), 1–11. doi: 10.1038/s41612-021-00190
 924 -x
- 925 Taylor, K. E., Stouffer, R. J., & Meehl, G. A. (2012). An Overview of CMIP5
 926 and the Experiment Design. *Bulletin of the American Meteorological Society*,
 927 *93*(4), 485–498. doi: 10.1175/BAMS-D-11-00094.1
- 928 Thompson, D. B., & Roundy, P. E. (2013). The Relationship between the
 929 Madden–Julian Oscillation and U.S. Violent Tornado Outbreaks in the
 930 Spring. *Monthly Weather Review*, *141*(6), 2087–2095. doi: 10.1175/
 931 MWR-D-12-00173.1
- 932 Ting, M., Kossin, J. P., Camargo, S. J., & Li, C. (2019). Past and Future Hurricane
 933 Intensity Change along the U.S. East Coast. *Scientific Reports*, *9*(1), 7795.
 934 doi: 10.1038/s41598-019-44252-w
- 935 Trapp, R. J., Diffenbaugh, N. S., Brooks, H. E., Baldwin, M. E., Robinson, E. D.,
 936 & Pal, J. S. (2007). Changes in severe thunderstorm environment frequency
 937 during the 21st century caused by anthropogenically enhanced global radiative

- 938 forcing. *Proceedings of the National Academy of Sciences*, 104(50), 19719–
939 19723. doi: 10.1073/pnas.0705494104
- 940 Trapp, R. J., Diffsenbaugh, N. S., & Gluhovsky, A. (2009). Transient response of se-
941 vere thunderstorm forcing to elevated greenhouse gas concentrations. *Geophys-*
942 *ical Research Letters*, 36(1). doi: 10.1029/2008GL036203
- 943 Weisman, M. L., & Rotunno, R. (2000). The Use of Vertical Wind Shear versus He-
944 licity in Interpreting Supercell Dynamics. *Journal of the Atmospheric Sciences*,
945 57(9), 1452–1472. doi: 10.1175/1520-0469(2000)057<1452:TUOVWS>2.0.CO;2
- 946 Zhang, G., & McFarlane, N. A. (1995). Sensitivity of climate simulations to
947 the parameterization of cumulus convection in the Canadian climate cen-
948 tre general circulation model. *Atmosphere-Ocean*, 33(3), 407–446. doi:
949 10.1080/07055900.1995.9649539
- 950 Zipser, E. J., Cecil, D. J., Liu, C., Nesbitt, S. W., & Yorty, D. P. (2006). WHERE
951 ARE THE MOST INTENSE THUNDERSTORMS ON EARTH? *Bulletin of*
952 *the American Meteorological Society*, 87(8), 1057–1072. doi: 10.1175/BAMS-87
953 -8-1057